Anthropogenic seismicity in Italy and its relation to tectonics: State of the art and perspectives

Thomas Braun[a], Simone Cesca[b], Daniela Kühn[b,c], Araksi Martirosian-Janssen[d], Torsten Dahm[b]

[a] *Istituto Nazionale di Geofisica e Vulcanologia, Roma, Italy*
[b] *Geoforschungszentrum-Potsdam, Potsdam, Germany*
[c] *NORSAR, Kjeller, Norway*
[d] *Institut für Geophysik, Universität Hamburg, Germany*

Abstract

Since hydrofracking is used for shale gas production, human caused seismicity have become a subject of increasing interest. Seismic monitoring is common for earthquakes generated by human operations like mining, reservoir impoundments, hydrocarbon and geothermal production, as well as reinjection of fluids. In Italy the M_w 6.1 Reggio-Emilia earthquake of 20$^{\text{th}}$ May 2012 triggered particular interest in anthropogenic seismicity. It also raised the question of whether hydrocarbon exploitation induced variations in crustal stress that influenced the generation of these earthquakes. The Italian government commissioned a technical report compiling cases of documented and hypothesized anthropogenic seismicity. This paper reviews these cases, on the basis of previously published works, and additional new analyses. Three cases of seismicity in Central Italy, occurring close to anthropogenic activities, are: (i) extraction of carbon dioxide (CO_2) from a borehole near Pieve Santo Stefano, (ii) the impoundment of the Montedoglio reservoir and (iii) geothermal energy production at Mt. Amiata. Since the sites are situated in the seismically active area of the Northern Apennines, we illustrate both by standard seismological analysis as well as by modeling to tackle the challenge of discriminating anthropogenic from natural seismicity.

Keywords: triggered/induced seismicity, Italy, CO_2 extraction, geothermal exploitation, reservoir impoundment, Mt. Amiata, Upper Tiber Valley

2017 MSC: 00-01, 99-00

1. Anthropogenic seismicity: an overview

1.1. Definition of induced, triggered and natural seismicity

Earthquakes represent a sudden mechanical instability and failure of rocks, releasing a part of the present internal shear stress. Almost all rocks carry pre-existing shear stresses, which have been generated by tectonic forces and mass movements. Additionally, internal stresses may be affected by humans and geotechnical operations. Therefore, under special conditions, earthquakes may be influenced or even caused by humans, which is defined as anthropogenic seismicity.

Almost all of the natural earthquake ruptures occur on pre-existing planes of weaknesses, i.e. geological faults. Pre-existing geological faults of different orientations and depths are present in nearly all hard rock formations of age, independent whether the region is far from or close to a plate boundary. However, only large fault systems are capable to develop earthquake ruptures large enough to morph into a strong and damaging earthquake. The largest faults are known to occur at plate boundaries, where they may evolve into rupture lengths of several hundreds or thousands of kilometers and rupture depths over the full brittle regime. Therefore, the largest tectonic earthquakes occur at plate boundaries, especially at subduction zones.

Except collapse earthquakes related to mining or subrosion sinkholes, anthropogenic earthquakes rupture in shear mode and release existing shear stress in the rock. Most likely, pre-existing faults are preferred rupture planes, especially if they are favorably oriented within the local stress field (e.g. Evans et al., 2012; Ellsworth, 2013), although anthropogenic earthquakes may in principle also rupture previously unbroken formations, e.g. within soft sediments. From a scientific viewpoint it is important to assess the maximum expected magnitude (M) in order to distinguish between stress changes completely generated by human actions, and the pre-existing stress within the formation. If the pre-existing shear stress on a fault is close to its critical level to rupturing, a relatively small portion of the fault affected by human-induced stress may lead to a large rupture plane, i.e. a large earthquake. Such an earthquake would be classified as triggered, because a large portion of the rupture was driven by pre-existing stress (e.g. McGarr et al., 2002; Dahm et al., 2013). On the other hand, if the pre-existing stress is below the critical level, the size of the human affected area of stress change constrains the size of the potentially generated earthquake, which is likely much smaller. Such an earthquake is termed induced, in the sense that the rupture has been driven exclusively by human-induced stress (Dahm et al., 2013).

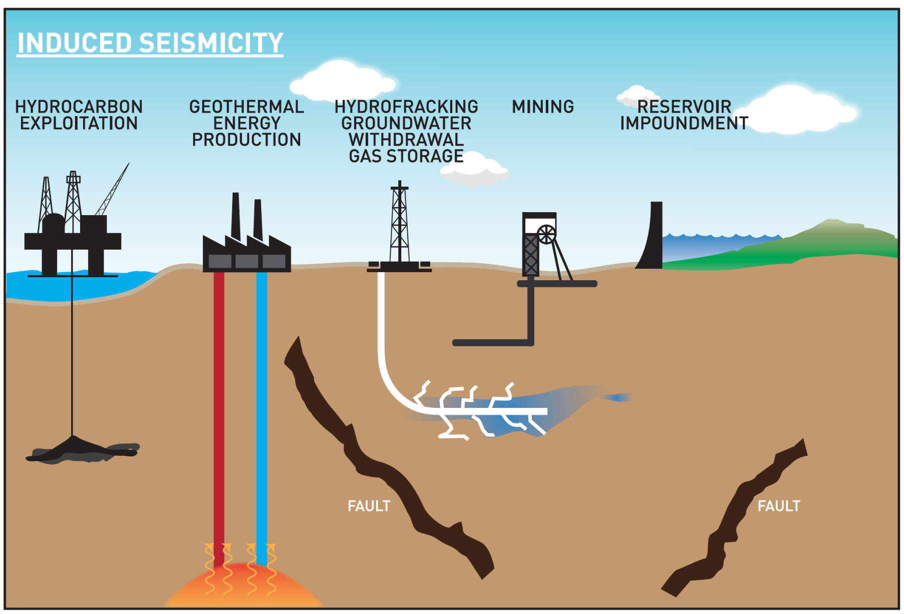

Figure 1: Possible causes of anthropogenic seismicity (modified from Ellsworth, 2013; Grigoli et al., 2017). Hydrocarbon exploitation comprises gas/oil production and wastewater injection; geothermal energy production includes vapour/water extractions and cold water reinjection.

Fig. 1 gives an overview of human geotechnical operations that may influence crustal stresses. They often deal with removal or injection of fluids at depth. This includes hydrocarbon exploitation, wastewater injection, fracking operations for unconventionals, the preparatory phase of an enhanced geothermal system, storage facilities for gas and oil, or groundwater withdrawal. Additionally, reservoir impoundment or excavation mining may influence crustal stresses. Earthquake rupture involves two physical processes: (i) the nucleation of the rupture process (trigger process) and (ii) the propagation of the rupture front and the growth of slip on the fault (rupture growth). The rupture nucleation can be influenced by pore pressure. Thus, if the pore pressure at depth is increased during a geotechnical operation, e.g. by injecting fluids in the subsurface, earthquake rupture may be triggered.

The rupture process (ii) defines the magnitude the earthquake may reach and is much more difficult to describe. Controlling parameters are again the level of dynamic Coulomb stress relative to the spatial distribution of the shear strength, additional to fault heterogeneities, geometrical complexities and temperature. Although it is still difficult to predict how large an earthquake rupture may grow after nucleation has occurred, the potential to grow into a large earthquake is given if the shear stress on the fault has reached a critical level. Otherwise, the rupture is arrested.

1.2. Types and examples of global anthropogenic seismicity

This section briefly reviews the relevance of anthropogenic seismicity worldwide in a context of the operations indicated in Fig. 1.

Mining activity may have generated seismic events already long before these events could be instrumentally recorded, since seismology is a comparatively recent field. The first monitoring network for mining induced seismicity was installed in the beginning of the 20^{th} century in the Ruhr district in Germany (Mintrop, 1909a,b; McGarr et al., 2002; Bischoff et al., 2010; Sen et al., 2013). Deep excavation mining, as coal- and potash salt mining, generated significant collapse earthquakes and rock bursts. Noteworthy are rock bursts, as e.g. the M_L 5.6 event with epicenter at Völkershausen (Germany), which was caused by the collapse of a potash mine and was felt within a radius of 300 km (Leydecker et al., 1998). Gold and coal mining has led to similarly strong earthquakes in the gold mine Orange Free State in South Africa with m_b 5.6, or coal mining events in Newcastle (1989, M_w 5.6) and Ellalong (1994, M_L 5.4), both in Australia (e.g. Davies et al., 2013). In 2016, two significant earthquakes occurred in a copper mine in Poland with magnitudes of M_L 4.5 and 4.6 (Lizurek et al., 2015; Rudzinski et al., 2015). In general, $M > 4$ events are not unusual in this mining district.

The first earthquake associated with reservoir impoundment was observed in 1932 at the Quedd Fodda Dam in Algeria. The first causal association between impoundment of a water reservoir and seismicity has been drawn during a study of Lake Mead in 1945 (Carder, 1945) and the first correlation between water level variations and earthquake rate was reported in 1949 for the reservoir impounded by the Hoover dam. Since then, reservoir induced seismicity has been observed at over seventy locations worldwide (Simpson, 1976, 1986; Gupta, 1992). Fortunately, no dam ever broke because of induced earthquakes.

Hydrocarbon production concerns the exploitation of gas and mineral oil, e.g. the extraction of methane from shallow gas reservoirs. The strongest events potentially related to long-term gas production were three $M > 7$ earthquakes at the Gazli gas field in Uzbekistan in 1976 and 1984 (e.g. McGarr et al., 2002; Davies et al., 2013). Other large earthquakes that are discussed in connection with induced or triggered seismicity are Coalinga 1983 (M 6.2), Kettleman North dome 1985 (M 6.1) and Whittier Narrows 1987 (M 6.0) (e.g. McGarr et al., 2002). Recently discussed events were much smaller in magnitude (e.g. Cesca et al., 2013b), as the M 4.8 earthquake 2011 near Fashing, Texas (Ellsworth, 2013), or the M_L 4.5 earthquake 2004 in Rotenburg, Germany (Dahm et al., 2007), the M 4.4 earthquake at the Cogdell oil field Snyder, Texas (Ellsworth, 2013), as well as the M 4.3 Ekofisk, North Sea event of 2001 (Cesca et al., 2011; Dahm et al., 2015). On 16$^{\text{th}}$ August 2012, an M_w 3.6 earthquake occurred in the Groningen field (Netherlands) causing considerable damages to homes in the area due to its shallow hypocenter. Relatively strong earthquakes related to gas production in France are known at Lacq gas field, with more than 2000 located events from 1974 to 1997 with $M_L \leq 4.2$ (e.g. Bardainne et al., 2008).

The production of oil and gas is often accompanied by the extraction of significant amounts of connate water. Mainly brines are trapped in sedimentary pore spaces and are brought to the surface while producing oil and gas. Since the 1930's much of this produced wastewater has been reinjected in disposal wells back into the producing reservoir in order to enhance hydrocarbon recovery by water-flooding operations. It is estimated that over 2 billion gallons of brine are injected in the United States (U.S.) every day, using approximately 20% of the 180,000 class II wells. Generally, reinjection into the sealed reservoir itself contributes to maintain reservoir pressure and to reduce reservoir depletion. However, reinjection is partly also realized into deep, open aquifer systems. There, fluid pressure may migrate over large lateral distances and into deeper basement faults and trigger earthquakes far away from the injection wells. Ellsworth (2013) compiled a list of seismicity related to wastewater injection in the U.S.; manifold are the cases of moderate earthquakes ($M > 4$), most of them reported from the U.S. midcontinent.

In Italy, the volumes of reinjected of wastewater are negligible with respect to the U.S.. The only noteworthy case is the Costa-Molina2-well in the Southern Apennines where maximum daily injection rates of 700 m^3/d are reached, inducing local seismic activity (Improta et al., 2015; Buttinelli et al., 2016, for details see section 2.3).

Hydrofracturing for unconventional shale gas extraction uses the controlled high-pressure injection of a fracking fluid (a mix of water, thicking agents, sand and other proppants) into a borehole to create tensile fractures that increase the permeability of the reservoir rock. This method is used since the 1950s to enhance the production capacity of tight gas reservoirs. With respect to wastewater injection, the involved fluid volumes during fracking are insignificantly small. The instrumentally recorded microseismicity consists accordingly of very small magnitude events ($M < 0$) and is not felt by humans. On the other hand, if the injected fluids lubricate an existing fault, higher magnitude events may be triggered and, considering the shallow operation depth, may lead to damages at the surface. The largest documented seismic event associated to hydrofracturing so far was the M_w 3.6 earthquake occurring 2009 in the Horn River Basin of British Columbia. Other more recent cases hypothesized to be related to fracking are reported from the Fox Creek area, Alberta (Canada); the strongest ones occurred on 25$^{\text{th}}$ August 2015 (M 4.6) and 12$^{\text{th}}$ January 2016 (M 4.8). The only known case of seismicity in Europe related to fracking was reported from Blackpool near Lancashire (United Kingdom) where fracking operations were stopped after a seismic M 2.3 event.

Hydrofracturing is also performed during operating Enhanced Geothermal Systems (EGS), formerly called Hot Dry Rock projects. To our knowledge, the largest earthquakes occurring during geothermal exploitation so far featured magnitudes below M_w 3.5, and have been observed in Switzerland in Basel (2006, M_w 3.4) and St. Gallen (2013, M_w 3.5), respectively (Deichmann and Giardini, 2009; Deichmann et al., 2014).

In Iceland, all reinjection sites in the high and low temperature geothermal fields are situated at plate boundaries and are characterized by an intense natural background seismicity. Any possibly induced earthquake vanishes in the high natural earthquake cloud and did therefore never alarm energy producers or the public. An exception was the strong seismicity recorded after starting voluminous reinjection at the power plant of Hellisheiði in 2011, causing intensive induced seismicity up to M 3.9, clearly felt in the nearby village of Hveragerði (Flovenz et al., 2015). Contrary to EGS, the operations performed during geothermal energy production usually involve only low pressures, with exception of the pressurized reinjection of cold fluids into the geothermal reservoir (e.g. Zang et al., 2014). Seismic events reported from such geothermal operations (e.g. California, Iceland, Australia, New Zealand; for more details on geothermal operations in Italy, see section 2.2) possessed magnitudes below M 4.0, except the M 4.6 earthquake recorded 1972 at "The Geysers" in the U.S..

Two other types of anthropogenic activity are continuous groundwater withdrawal and gas storage. Gonzáles et al. (2012) suggested that the deadly M 5.1 earthquake occurring on 11$^{\text{th}}$ May 2011 at Lorca (Spain), could have been triggered by continuous groundwater withdrawal, unloading a crustal volume close to an active fault. Cases of seismicity related to CO_2 storage are reported by Nicol et al. (2011) (and references therein). Depleted oil and gas reservoirs lend themselves both to capture and sequestration of CO_2 - carbon capture and storage (CCS) - as well as to seasonal storage of methane. In Europe, CCS is only realized in the remotely situated Sleipner off-shore gas field (250 km west of Norway), with no reports of stronger seismic events so far. Seismic monitoring near the CCS demonstration site in Illinois reveals occasional swarm-like microseismicity with magnitudes $M < 1.5$ (Kaven et al., 2015). Temporary methane storage at the CASTOR site (22 km off the coast of Spain) was suspected to be responsible for a sustained seismic sequence, culminating in a M 4.3 earthquake in October 2013 (Cesca et al., 2014; Gaite et al., 2016). From Italy, where seasonal storage of methane is practiced since decades, no significant seismicity was reported. An updated overview of anthropogenic seismicity in Europe, is given by Cesca et al. (2013b) and Grigoli et al. (2017).

2. A review of anthropogenic seismicity in Italy

In Italy, up to now the number of documented and hypothesized cases of triggered and induced seismicity is relatively small (Tab. 1).
In 2014, the Superior Institute of Environmental Protection and Research (ISPRA, 2014) published a report on triggered or induced seismicity in Italy, distinguishing four main types of documented (doc) or hypothesized (hyp) cases: impoundment of reservoirs (res), geothermal exploitation (geo), hydrocarbon extraction (ext), wastewater reinjection (rei) and mining (min).

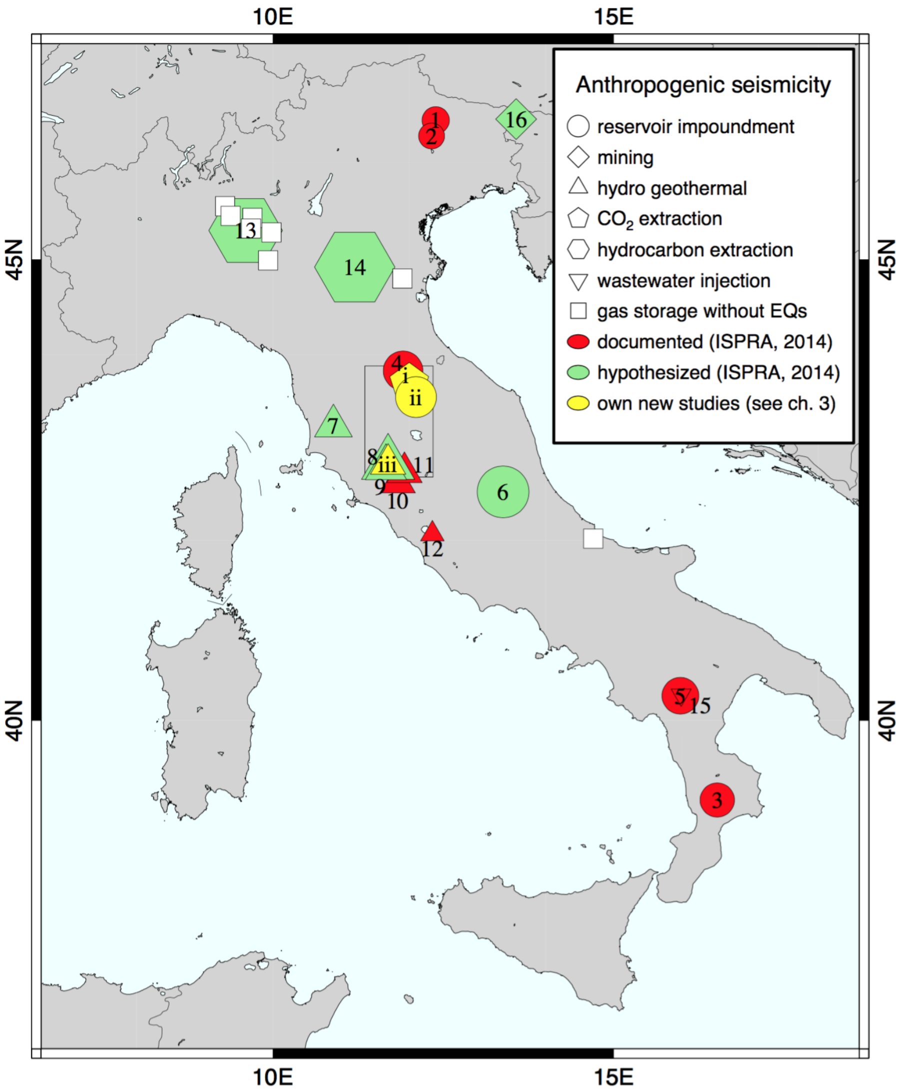

Figure 2: Seismicity in Italy related to anthropogenic activity: (1-16) treated in ISPRA (2014), see Tab. 1; (i-iii) analyzed in this study, inside the rectangular area (see section 3).

In the following section, we revisit the examples given in Tab. 1 and discuss their origin both based on previous studies (section 2), as well as on our own work (section 3, Fig. 2).

n	activity	$Lon°$(E)	$Lat°$(N)	M_{max}	year	I_{MCS}	Location
1	res doc	12.39	46.43	2.0	1964		Pieve di Cadore
2	res doc	12.33	46.27	1.9	1963		Vajont
3	res doc	16.52	39.10	2.5			Passante
4	res doc	11.91	43.83	2.9	1989		Ridracoli
5	res doc	15.98	40.28	2.7	2010		Pertusillo
6	res hyp	13.38	42.53	5.7	1950	8	Campotosto
7	geo hyp	10.89	43.24	3.2	1978		Larderello/Travale
8	geo hyp	11.69	42.83	4.5	2000	6	Amiata
9	geo hyp			3.5	1983		Amiata
10	geo doc	11.83	42.63	3.0	1984		Latera
11	geo doc	11.93	42.74	3.0	1977	3/4	Torre Alfina
12	geo doc	09.15	45.63	2.0	1978		Cesano
13	ext hyp	09.60	45.30	5.4	1951	6/7	Caviaga
14	ext hyp	11.20	44.92	5.9	2012	7/8	Cavone
15	rei hyp	15.99	40.29	1.7	2006		Montemurro
16	min hyp	13.57	46.44	n.d.	1965	5	Raibl/Cave Predil

Table 1: Suggested human-related earthquakes in Italy. Geographical coordinates, magnitude, intensity Mercalli-Cancani-Sieberg scale (MCS), and location of human activities: **hyp**othesized and **doc**umented cases of triggered or induced seismicity related to **res**ervoir impoundment, **geo**thermal exploitation, **ext**raction and **rei**njection of hydrocarbons, **min**ing (after ISPRA, 2014).

2.1. Reservoir induced and triggered seismicity

The first researcher in Italy expressing the idea that seismic events can be generated by human activity was Caloi (1970). From seismic observations of only a single station installed on top of the Pieve di Cadore dam (Italian alps), Caloi and Spadea (1966) reported the recording of tens of thousands of microseismic events ($M \leq 2$) during the first five years after construction and proposed both seasonal and diurnal temperature variations as well as variations of the water load as potential causes.

A further example studied by Caloi (1966) was the Vajont dam (Italian alps), famous for the disastrous landslide of 9$^{\text{th}}$ October 1963 with at least 1910 victims. He reported a significant correlation between the rise of the water filling level and the increase of seismic activity, both before and after the rockfall (Caloi, 1970). Even if the observations consisted solely of the recordings of a single station, the observed S-P travel time differences allowed to deduce approximate event locations.

Giuseppetti et al. (1996) report a M 2.5 earthquake close to the Passante dam in Calabria, but offer no record about potential damage.

Significant seismicity related to the filling of an artificial lake was reported from of the Ridracoli reservoir (Northern Apennines). The area is characterized by historic earthquake activity with intensities up to $I_{MCS} = IX - X$ (Mercalli-Cancani-Sieberg scale; Boccaletti et al., 1985). During the 1980s, a six-station seismic network was installed and Piccinelli et al. (1995) report a significant correlation between water level and seismicity rate ($0.8 \leq M \leq 2.8$) within a distance range of 5 km from the dam, indicating a 60-day time lag between maximum reservoir water level and occurrence of local microseismicity. This delayed or so-called drained response was interpreted to be generated by pore pressure diffusion and water flux outside the basin coupled to the load, rather than to pore pressure increase due to load variations.

A recently published example of reservoir induced/triggered seismicity concerns the Val d'Agri extensional basin, an area with one of the highest seismogenic potentials in Italy (M 7.0 in 1857). Valoroso et al. (2009) analyzed about 2000 microearthquakes ($-0.2 \leq M_L \leq 2.7$) recorded by a dense network during a 13-months-lasting seismic experiment. They found a temporal correlation between the intense microseismicity and the loading and unloading phases of the Pertusillo dam situated nearby.

After the M_w 6.3 L'Aquila earthquake in 2009, Mucciarelli (2013) called the attention to a possible link between significant historical earthquakes occurring nearby the artificial Campotosto lake, situated only 20 km to the northwest with respect to the epicenter of the 2009 main shock. Mucciarelli (2013) suggested that damaging seismic events ($I_{MCS} > VI$) during the last century located near the Campotosto lake (Locati et al., 2016) are concentrated temporally during the fifties, reaching a maximum magnitude of M 5.7. Even if - due to the sparseness of the former seismic monitoring network - the epicentral location errors might amount to an order of tens of kilometers, it is noticeable that the earthquakes occurred exactly during the period of construction and impounding of the reservoir. Mucciarelli (2013) proposed therefore to not exclude a priori the possibility that the recent activity on the Campotosto fault could also be influenced by anthropogenic activity.

2.2. Geothermal fields

Apart from Iceland, the main high-temperature geothermal areas of Europe are all situated in Central Italy. Located westwards of the high-angle normal faults of the Central Apennines, the geothermal areas of Larderello, Mt. Amiata, Latera, Torre Alfina, and Cesano are characterized by moderate seismicity (Batini et al., 1980a,b, 1985, 1990; Evans et al., 2012; Moia et al., 1993; Mucciarelli et al., 2001).

Damaging earthquakes struck the geothermal areas in South Tuscany long before geothermal exploitation started in the 1950s (Braun et al., 2016). The Parametric Catalog of Italian Earthquakes (CPTI) (Locati et al., 2016) reports as highest magnitudes during the last century a M_e 5.32 event in 1919 near Mt. Amiata and a M_e 4.93 event in 1957 at Castel Giorgio. Both locations as well as magnitude calculations are afflicted by large errors due to the sparse configuration of the recording seismic monitoring network. Recently observed seismic events, as the M_L 4.1 seismic event occurring on 30$^{\text{th}}$ May 2016 near the abandoned geothermal production field of Torre Alfina, give testimony of continuous natural stress relaxation by earthquakes (Braun et al., 2018).

The strongest earthquake in recent times occurred on 1$^{\text{st}}$ April 2000 and had a magnitude of M_L 3.9/M_w 4.5 (Castello et al., 2006), raising strong concern among the general public. Its shallow hypocentral depth was responsible for generating a peak ground acceleration of 147 cm/s^2, damaging more than 50 buildings at Piancastagnaio, mostly old stone masonry houses with poor anti-seismic behavior (Mucciarelli et al., 2001). The proximity of macroseismic epicenter and geothermal power plant raised strong doubts about the natural origin of this earthquake.

Due to the lack of adequate data, up to now a reliable hypocentral depth determination of this strongest earthquake ever recorded in an Italian geothermal area, was not possible. In section 3.3, we present new analyses of the 1$^{\text{st}}$ April 2000 event, using for the first time data from a local seismic network operated and made available by the national electricity producer ENEL-Greenpower.

2.3. Hydrocarbon extraction and reinjection of wastewater

On 15$^{\text{th}}$ and 16$^{\text{th}}$ May 1951, two seismic events with magnitudes of M_w 5.4 and M_w 4.5 occurred about 40 km southeast of Milan North Italy close to the location of Caviaga, an area that was formerly assumed to be aseismic. For these earthquakes, Caloi et al. (1956) reported a hypocentral depth of 5 km, and pointed out the possibility that they could have been related to well operations for gas withdrawal. Considering that in the 1950s, the national Italian seismic monitoring network consisted of about 20 seismic stations and that at that time neither a reliable velocity model was available nor any background knowledge about regional historical seismicity, the Caviaga events where included in the ISPRA-report as hypothetically induced (Tab. 1; ISPRA, 2014). Recently, Caciagli et al. (2015) re-examined these events using historical macroseismic and seismic data. Earthquake relocation, by using updated crustal velocity models and location routines, revealed hypocentral sources at mid-crustal depths, much deeper than the production level of the hydrocarbon exploitation. Consulting the CPTI (Locati et al., 2016) allowed to identify significant historical seismicity in the area, both facts being strong indications for the natural tectonic rather than anthropogenic origin of the 1951 earthquakes.

The seismic event that triggered the current interest in anthropogenic seismicity in Italy was the M_w 6.1 Reggio-Emilia earthquake on 20$^{\text{th}}$ May 2012, which caused - together with the second M_w 5.9 main shock on 29$^{\text{th}}$ May 2012 - 27 victims and rendered 1500 people homeless (Cesca et al., 2013a). Since the area is subject to intensive hydrocarbon exploitation since the 1950s, the question arose whether hydrocarbon exploitation at Cavone could have induced or triggered the seismic sequence. An International Commission on Hydrocarbon Exploration and Seismicity in the Emilia-Romagna region (ICHESE, 2014) was convoked to investigate a potential relationship between human activity and the Emilia earthquakes. The ICHESE-commission reasoned that the Cavone oilfield and the Casaglia geothermal field were the only possible areas of hypothetic anthropogenic activity, concluding that the anthropogenic stress change was most likely too small to have induced a seismic event, but that a triggering cannot be excluded.

Several studies followed, using either field studies (e.g. the Cavone Monitoring Lab) or numerical modelling (e.g. Astiz et al., 2014; Dahm et al., 2015).

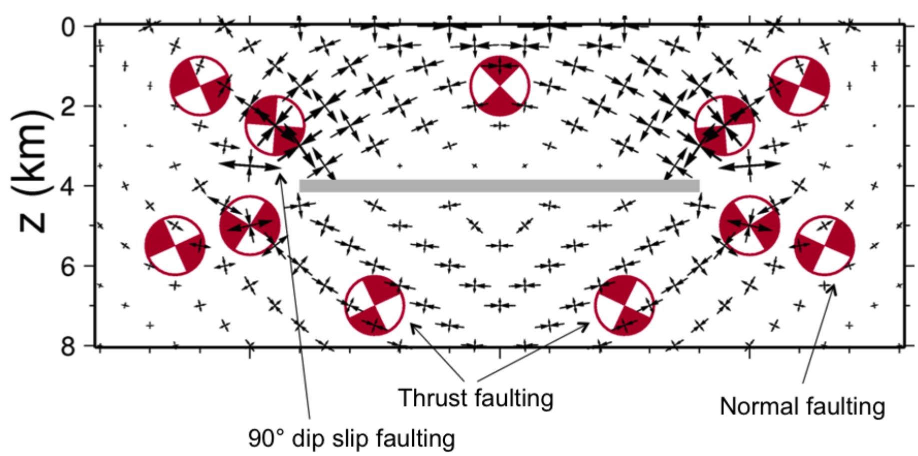

Figure 3: Depth section of a hypothetic depleted hydrocarbon reservoir (gray horizontal bar) situated at a depth of 4 km. Arrows indicate the main stress components and red beach balls the corresponding double couple mechanisms. Normal faulting is expected at the depth level of and sidewards from the reservoir, whereas thrust faulting is supposed to occur above and below the reservoir.

Dahm et al. (2015) found clear indications that the Emilia events in 2012 were neither induced nor triggered by depletion of the oil field, and that both earthquakes are exclusively of tectonic origin. Justifications for this conclusion are the distance of about 20 km between main shock and Cavone oil field, the minor pore pressure reduction during the lifetime of its exploitation as well as the unfavorably oriented mechanism (Fig. 3).

The third example of hypothesized anthropogenic seismicity related to hydrocarbon exploitation is a wastewater injection near the location of Montemurro (Val d'Agri). The Val d'Agri basin is situated in the southern Apennines and hosts the largest on-shore oil field in Europe. The largest earthquake ever recorded in this area had a magnitude of M 7.0 (1857) (Valoroso et al., 2009; Improta et al., 2015), attesting the Val d'Agri a high seismic hazard. From 2006 on, wastewater extracted during hydrocarbon exploitation was continuously reinjected in the Costa-Molina2 well into an unproductive marginal portion of the carbonate reservoir at the well bottom at 3 km depth (Improta et al., 2015; Buttinelli et al., 2016).

Seismicity related to the reinjection was first investigated by Valoroso et al. (2009) and Stabile et al. (2014). In a detailed analysis Improta et al. (2015) reported that in June 2006 intense microseismicity (111 events with $M \leq 1.8$) was recorded 1 km below the well-bottom on a formerly inactive blind fault three hours after the start of the injection of wastewater into a high rate well. The rate of seismic event occurrence and the cumulative number of earthquakes strictly correlated with wellhead pressure and injection rate, reaching maximum values of 13-14 MPa and 2800 - 3000 m^3/d. High precision location of 219 events ($M_L \leq 2.2$) occurring between 2006 and 2013 revealed both, a strong correlation of the seismicity with short-term variations of the injection pressure, as well as the concentration of hypocenters on the same newly activated blind fault (Improta et al., 2015).

2.4. Mining

The last category of potential sources for anthropogenic seismicity mentioned in the report by ISPRA (2014) is mining. Mucciarelli (2013) report only one historical event, in the northeastern part of Italy exhibiting a maximal intensity of $I_{MCS} = V$. In 1965, an earthquake occurred at the Raibl mine close to the village Cave del Predil causing three deaths and four injuries among miners and damages to the buildings. It was again Caloi (1970), who attributed this event to human activity, leading to include this seismic event as hypothetically induced in the report by ISPRA (2014).

3. Three new case studies from the Apennines

Tuscany is the location of a series of interesting seismogenic phenomena (Fig. 4): the geothermal areas of Larderello and Mt. Amiata (Braun et al., 2016), a large CO_2 reservoir (Heinicke et al., 2006) and a huge reservoir impoundment on top of the earthquake generating Alto Tiberina Fault (ATF) system (Braun et al., 2015). The ATF has also been suggested to experience aseismic creep as well as episodes of non-volcanic tremor (Saccorotti et al., 2011). In the following section, we present three new case studies of seismicity observed near anthropic activities:

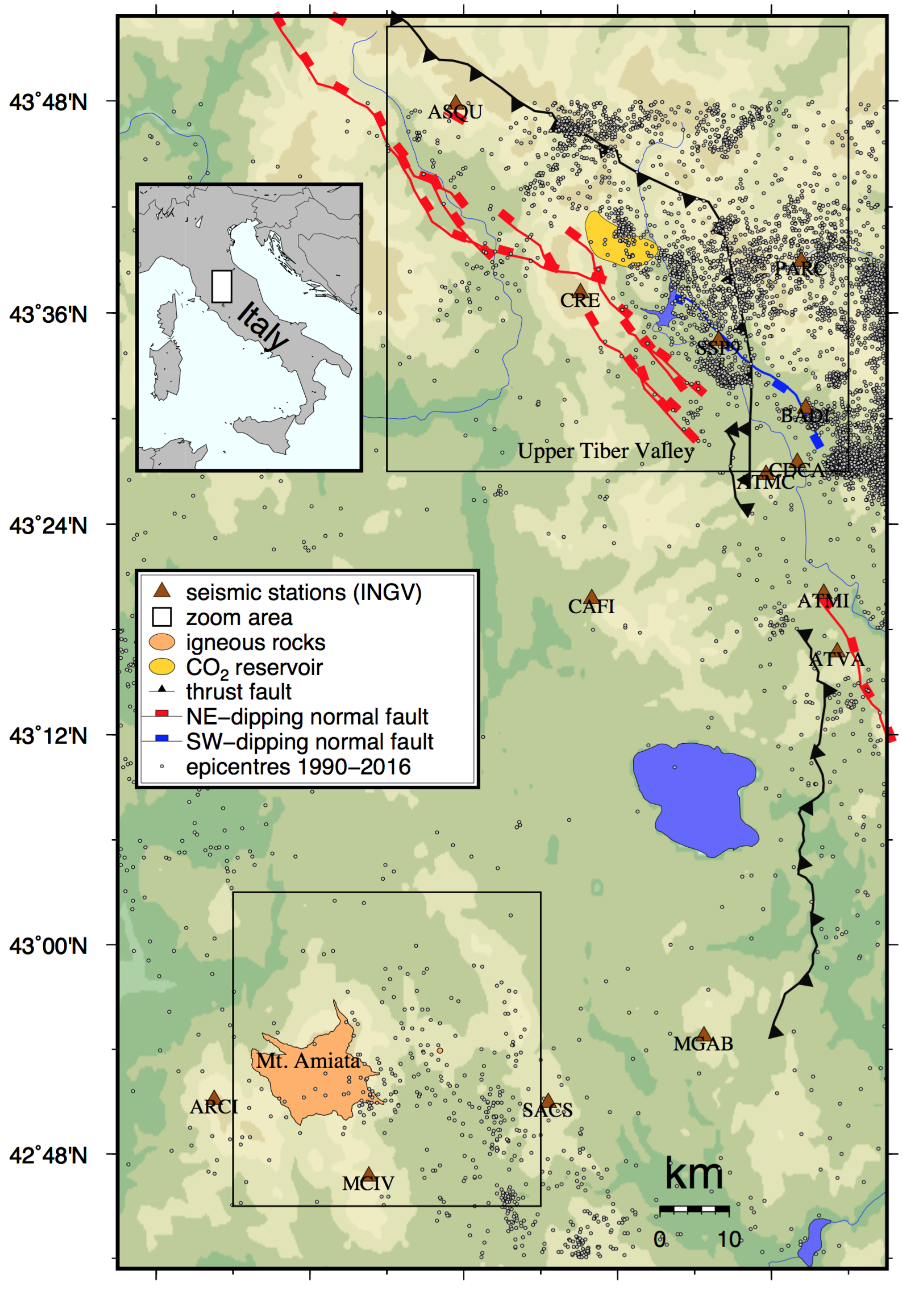

Figure 4: Location of the areas investigated in the present contribution: Upper Tiber Valley (NE) CO_2 production (section 3.1; Fig. 5 and reservoir impoundment (section 3.2); Mt. Amiata (SW) geothermal exploitation (section 3.3; Fig. 9). Main faults, Seismicity (1990 - 2016) and the seismic network of INGV are illustrated (see legend for symbols).

i. the production of CO_2 from the borehole near Pieve Santo Stefano (PSS)

ii. the impoundment reservoir of Montedoglio (Upper Tiber Valley)

iii. geothermal energy production at Mt. Amiata.

Since all three examples are located in Tuscany, a short introduction about the regional geology will precede the data analyses.

As a result of the extensive tectonic evolution, the Northern Apennines are divided into two domains with different geological and geophysical characteristics: the *Tyrrhenian* (western) and *Adriatic* (eastern) domain (Barchi et al., 2003). Recent analyses of GPS-data by Hreinsdóttir and Bennett (2009) show that in the northern part of the Central Apennines both domains deflect relatively by creeping (~ 2 mm/a). The contact zone of the extensional regime falls close to the well-known structure of the seismically active ATF, a NNW-SSE striking fault system composed of a ENE-dipping low-angle normal fault and its antithetic WSW-dipping high-angle normal fault, both active since the Late Pliocene (Boncio et al., 2000; Collettini and Barchi, 2003).

Focal solutions of the most important earthquakes occurring in the Central Apennines are predominately NNW-SSE-striking normal faults (Chiaraluce et al., 2007). Analysis of seismic episodes, observed directly north of the CROP-03 profile (Fig. 5), as e.g. the seismic sequence following the M 4.4 event on 26$^{\text{th}}$ November 2001, reveals however similar hypocentral distribution and a mainly normal focal mechanism as for the ATF. These observations suggest that the ATF-system continues also N of the CROP-03 profile (Piccinini et al., 2009) up to the Montedoglio reservoir and the area of CO_2 degassing near the PSS-borehole (Fig. 5).

3.1. Seismicity observed near a CO_2 *production site*

The first case study concerns the industrial extraction of CO_2 in the Upper Tiber Valley (UTV). The area between Caprese Michelangelo and Pieve Santo Stefano is characterized by several natural superficial cold CO_2 springs (mofettes), often accompanied by rain water emersion, resembling to mud volcanoes (see Heinicke et al., 2006, and references therein). In Italy, such phenomena are widespread and have been extensively described by many studies. Chiodini et al. (2004) explain the occurrence of degassing by mantle uplift in the western part of the Apennines; mantle fluids are rising into the ductile upper crust under nearly lithostatic pressure and diffuse through the thrust faults, forming vents and mofettes at the surface. They report that the western part of central and southern Italy is covered by venting areas, most of them are of volcanic origin, but there are also geothermal areas and non-volcanic emissions. One of those areas is called Fungaia, situated near Caprese Michelangelo. Beneath Fungaia, a natural CO_2 reservoir in 3.8 km depth has been identified (Anelli et al., 1994). A possible relation of CO_2 degassing and the occurrence of earthquakes in regional distance was proposed by Heinicke et al. (2006).

In order to monitor the microseismic activity connected to the anthropogenic activity of CO_2 production from the Fungaia reservoir, we deployed a seismic array near the small town of Caprese Michelangelo (CAMI, Fig.5) in 2010, as integration of the already existing seismic network (Braun et al., 2004). Main objective was to discriminate natural from anthropogenic seismicity possibly generated by the industrial operations. The CO_2 reservoir beneath Fungaia, already explored in the 1980s by drilling the 5 km deep PSS-borehole (Fig. 5), was scheduled to be industrially exploited after 2011. Since it could be expected that the production would cause a slow depletion of the reservoir, the resulting pore pressure change might influence the seismicity rate. To study in detail the characteristics of the local seismicity before, during and after the industrial activity a small aperture seismic array was installed already one year prior to the beginning of the exploitation. The only noteworthy seismic activity was recorded during August 2010, one year before the flush production. The seismic sequence comprised 34 events, the strongest reaching M_L 3.2. The hypocenters cluster few kilometers inside the reservoir along its northeastern external border.

Our analysis focused on two small earthquake swarms recorded (a) during August 2010 and (b) between July and September 2011. In a first approach, the overall 151 events were located employing the location routine HYPOSAT

(Schweitzer, 2001) using the best regional minimum 1D velocity model proposed by Piccinini et al. (2009) (Fig. 5). To improve hypocentral locations, the events were relocated with the HypoDD-code, based on the double-difference earthquake location algorithm (Waldhauser, 2001; Waldhauser and Ellsworth, 2000). A notable alignment of the relocated cluster in apenninic direction (NW-SE) is obvious (Fig. 5). Although the relocation was very addicted to single events due to their relative dependency, resulting in horizontal shifting of the cluster from the absolute location, both routines resulted in the same depth level of about 5 km, both below the reservoir as well as below the ATF, the re-located cluster appears to be situated closer to the ATF's eastern descending border.

Concerning the second swarm (b) occurring between July and September 2011, the magnitudes of the recorded events were too small to be recorded by seismic stations outside the array.

Two of the clusters occurred at similar depth as the August 2010 earthquake swarm, while the third one was located in a deeper range of 12 - 14 km, which is quite interesting, since there are no known faults or sources in these depths. The focal mechanisms for the strongest events of August 2010 (M_L 3.2, M_L 3.0, M_L 2.9) were calculated both using P-polarities, as well as by fitting full waveform amplitude spectra according to Cesca et al. (2010). Unexpectedly, all three focal mechanisms, located in 6 - 7 km depth along the NW-border of the reservoir (Fig. 5), show thrust faulting mechanism with an Apenninic strike, in an area where normal faulting is predominant (Fig. 5).

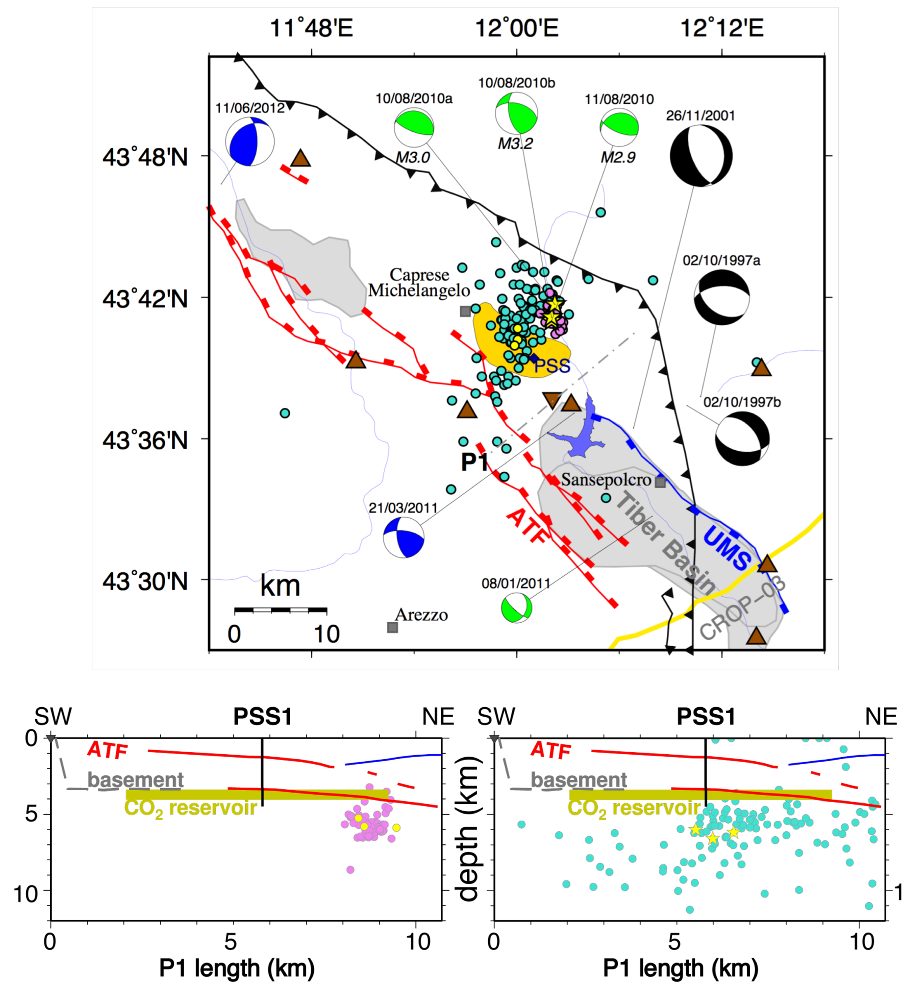

Figure 5: (Up:) Overview of the working area near the CO_2 reservoir (yellow area): the blue diamond indicates the PSS-well, brown and inverted triangles represent the location of the seismic stations and the CAMI-array, respectively. Circles depict the absolute earthquake locations (cyan) and the HypoDD solutions (magenta) of the August 2010 earthquake swarm; the three strongest events $2.9 \leq M \leq 3.2$ are plotted as yellow stars. Moment tensor solutions resulting from the present study are: (i) upper mantle thrust fault mechanisms ($M > 3$ in blue), (ii) upper crustal events (green), three thrust solutions $2.9 \leq M_L \leq 3.2$ and one normal fault (08/01/2011) (section 3.2); typical upper-crustal normal fault mechanisms of the UTV ($M > 3$ in black, Piccinini et al., 2009)). (Down:) Depth projection on the anti-apenninic depth profiles P1 of the HypoDD relocations *(left)* and the absolute locations *(right)*.

Accidentally, our attention turned to two deep-focus earthquakes, reported in the ISIDe bulletin at depths of z> 50 km. We relocated these formerly never analyzed earthquakes, i.e. (i) the M_L 3.1 event of 21st March 2011 and (ii) the M_L 3.7 earthquake of 11th June 2012, and calculated the corresponding moment tensors using the routine by Cesca et al. (2010). We confirm that both events are located in the upper mantle at hypocentral depths of (i) z = 55 km and (ii) z = 68 km, respectively, and find that both show a clear thrust component, being probably related to the slab (Fig. 5).

The location of the M_L 3.2 event at the border of the reservoir and its inverse mechanism, leads us to the following conclusions:

- The events beneath the CO_2 reservoir did not exceed M 3.2 prior to production.

- The three main events with $2.9 \leq M_L \leq 3.2$ indicate reverse faulting in an area which has been classified by extensional tectonics and the occurrence of normal-faults.

- A direct relation of the seismicity and the gas extraction could not be found. The events occurred before starting the extraction activity. Furthermore, we find unusual source mechanism for the events. These points lead to the assumption that the August 2010 events occurred under compressional stress, indicating a possible rotation of stress axes beneath the ATF, which possibly serves as a stress decoupling zone. Elsewhere, a stress decoupling has been observed for weak layers (e.g. salt) in sedimentary basins, or at creeping fault zones.

We conclude that the stress conditions of the reservoir at depth are likely decoupled from stress in the shallower layers. The internal conditions of overpressure in the gas reservoir may play an additional role to change effective stresses. The fact that these earthquakes occurred before starting the CO_2 production excludes any anthropogenic influence. However, if this "natural" seismicity would have taken place some months later, they probably would have been interpreted as "induced" or "triggered".

3.2. Seismicity near the Montedoglio reservoir

The second case study investigates a potential relation between water level changes in the Montedoglio reservoir located at the northern boundary of the Tiber basin very close to the ATF and the local seismicity. Fig. 4 (Upper Tiber Valley zoom area) shows that most of the seismicity since 1983 close to the Montedoglio reservoir occur at shallow depth of less than 10 km on or in the hanging wall of the ATF, where the Montedoglio reservoir is located as well. Since both tectonic processes at the ATF and water level changes in the reservoir may influence the local stress field, it is challenging to discriminate reservoir induced from reservoir triggered or tectonic events.

The strongest events ($M > 4$) potentially associated with the changes in the water reservoir occurred on the 2nd Oct 1997 and the 26th Nov 2001, respectively. Their normal faulting focal mechanisms obtained from P-wave polarities are depicted in black in Fig. 5 (Piccinini et al., 2009). Further, focal mechanisms are shown for events on the 8th January 2011 and the 21st March 2011 (plotted in green and blue). These events follow a failure of the dam crest on the evening of the 29th December 2010 (Fig. 6).

An initial outflow of 700 m^3/s was recorded, which reduced the water volume in the reservoir by 40%, corresponding to a volume loss of 55 Mio m^3. As illustrated in Fig. 6, the failure of the dam crest caused a water level drop of 14 m within eight days (corresponding to a pressure drop of 1.4 bar), regorging enormous water masses towards the valley. During the following three months two earthquakes occurred in direct vicinity of the Montedoglio reservoir: on the 8th January 2011, a M 2.3 event was recorded at a depth of 8 km and a lateral distance of 7.5 km southeast of the dam (occurring within a sequence of seven events) and on the 21st March 2011, a M 3.1 event occurred close to the dam, but at a depth of 55 km.

However, the 8th January 2011 event features a normal faulting mechanism typical for the ATF, with a strike direction matching the Apennines (Fig. 5).

The large hypocentral depth together with the strong thrust component of the 21st March 2011 event indicates an activation of a deeper structure that is independent from the ATF (Fig. 5). Since their relatively large hypocentral distance to the reservoir renders triggering by the volume variation of the Montedoglio reservoir unlikely, both 2011 events are disregarded in the following discussion.

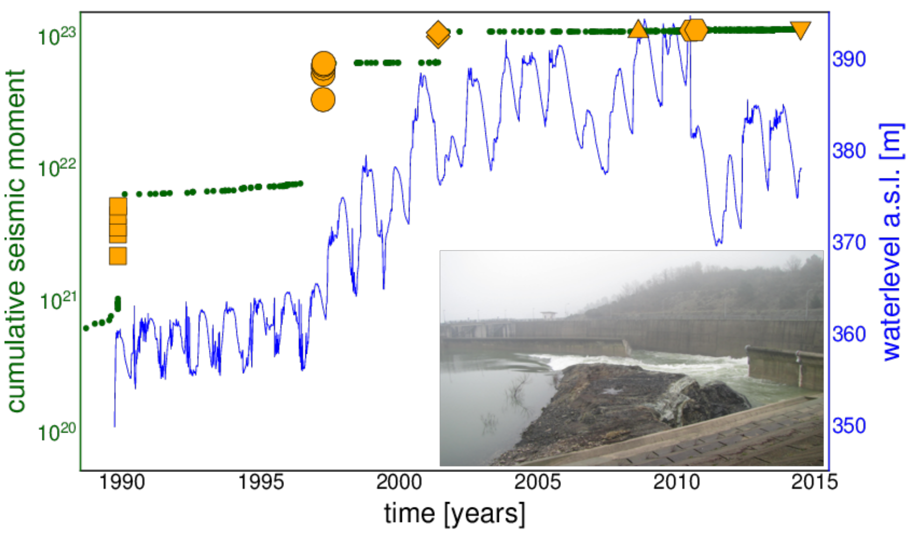

Figure 6: Temporal variations of the water level (blue line) compared with the cumulative seismic moment (green dots) recorded for events occurring inside the specified 20 km x 20 km area. Orange symbols represent the 16 largest events occurring in 1990 (squares), 1997 (circles), 2001 (diamonds), 2009 (triangles), 2011 (hexagons) and 2014 (inverted triangles); (inset) photograph of the rupture of the dam crest in the evening of the 29th December 2010.

Reservoir induced seismicity is supposed to result both from the instantaneous effect due to the elastic and undrained response to loading (or unloading) as well as the delayed effect due to the drained response and pore pressure changes by diffusion (Talwani, 1997). In the following, we will discuss both mechanisms on the basis of the Montedoglio reservoir.

For our analysis, we defined an area of 20 km x 20 km surrounding the Montedoglio reservoir. Fig. 6 illustrates a comparison between the cumulative seismic moment, the 16 largest events within that region and the water level changes from the start of impoundment in 1990 to 2014. Locations and origin times of these events are given in the electronic supplement (ES) Tab. 3. The harmonic oscillations of the water level are due to seasonal changes (high water level in winter, low water level in summer). Apart from seasonal variations, fig. 6 shows six significant water level changes:

- the beginning of impoundment in 1990,
- a strong increase in autumn 1997,
- a significant filling rate decrease at the end of spring 2001,
- a stronger increase of the water level than during the previous years during the winter season 2008/2009,
- a sudden decrease caused by the failure of the dam crest in Dec. 2010,
- and a sudden decrease of the water level in 2014.

It is easily visible that the occurrence of the largest events fits these changes in water level. Five important seismic sequences have been recorded shortly after these major impoundment changes took place: (a) in May 1990 (maximum observed magnitude M 3.2), (b) in October 1997 (maximum observed magnitude M 4.2), (c) in November 2001 (maximum observed magnitude M 4.3), (d) in February 2009 (maximum observed magnitude M 3.0), and (e) in December 2014 (maximum observed magnitude M 3.6). The progression of earthquakes in the ES-Tab. 3 indicates an apparent increase in magnitude of events close to the reservoir between 1990 and 2001 (M 3.2 on $8^{\text{th}}/9^{\text{th}}$ May 1990, M 4.2 on 2^{nd} October 1997, M 4.3 on 26^{th} November 2001) potentially correlating with the long-term increase of the reservoir's water level. However, the trend in magnitude evolution is not very strong and there are exceptions. An expected pattern for reservoir induced earthquakes is that seismicity occurs only after previous pressure levels have been significantly exceeded. This can be explained by the so-called Kaiser-effect or stress shadow effect (Kaiser, 1950). Such a pattern may be present in the Montedoglio sequence for larger magnitude earthquakes.

To test this hypothesis, we will analyze the time delay between the exceedance of the stress shadow of the previous loading and the occurrence of the events.

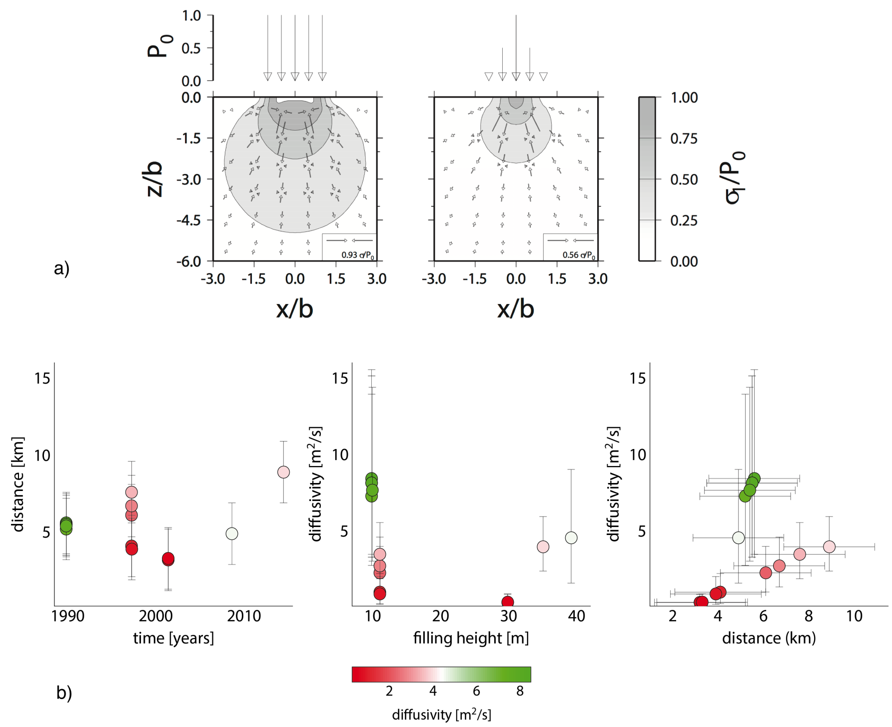

Figure 7: a) Stress distribution in the subsurface due to the pressure resulting from a homogenous (left) and triangular (right) static load P_0 (water column height) at the free surface. The arrows and contour lines display the direction and normalized magnitude of σ_1 (maximum compression). Vertical (z) and horizontal (x) dimensions are normalized relative to (b) - the reservoir dimension. b) Comparison of earthquake characteristic and hydraulic parameters; left: hypocentral distance of earthquakes to lake shore over time, middle: seismic hydraulic diffusivity compared to filling height of reservoir, right: seismic hydraulic diffusivity with distance to reservoir; circles colored according to seismic hydraulic diffusivity.

But first, in order to understand the elastic and undrained response, we modeled the crustal stress variations expected from the static load of the water column and compared it to the local seismicity. We use analytical 2D stress field solutions of a uniform and a pyramid-shaped strip load acting on an elastic half-space. The solutions are based on Flamant's problem for a line load on an elastic half space (e.g. Davis and Selvadurai, 1996; Dahm, 2000, in appendix A). Fig. 7 shows the normalized stress as a function of distance and depth from the center of the reservoir load at the surface.

For instance, a level change of 10 m generates a pressure change at the surface of about $P_0 = 0.1$MPa. Assuming a lake width of 3 km, the maximum compressive stress has already decreased to 0.025 MPa (to $P_0/4$) at a depth of 3.75 km beneath the reservoir or in a horizontal distance of 2.25 km from the center of the reservoir for the pyramid-shaped strip load. For a uniform loading pressure over the entire width of the reservoir, the estimated attenuation depth and distance increase to 7.5 km and 4 km, respectively. We conclude that lake level variations of 10 m induce rather small instantaneous stress changes at the distances of occurrence of the larger earthquakes. In addition, the time lag between significant water level changes and the occurrence of larger magnitude earthquakes hints to the importance of pore pressure changes due to fluid diffusion as triggering mechanism.

In order to study the influence of pore pressure diffusion, we estimated the seismic hydraulic diffusivity α_S according to $\alpha_S = L^2/t$ (Talwani and Acree, 1985) from the origin time and location of the events. As distance measure L, we employed the hypocentral distance of events to the lake shore. In most cases, we measured the time t as period between the day, where the previous maximum filling level of the reservoir was exceeded and the occurrence time of the events. However, we allow for the following exceptions: in 1990, we assumed t as the time between the start of impoundment and the occurrence of events. Since in 2007, the water level decreased to the lowest level since the year 2000, we compute the time t as days between the exceedance of the highest water level in 2008 and the occurrence of events in 2009. The results are listed in the ES-Tab. 4.

Hydraulic diffusivity values for this region given in literature differ widely. Antonioli et al. (2005) extract hydraulic diffusivity values of 22 - 90 m^2/s from the temporal evolution of the 1997 Umbria-Marche seismic sequence with an anisotropic diffusivity of 250 m^2/s along faults. Heinicke et al. (2006), analyzing the connection between temporal variations in fluid expulsions at the mofettes of Caprese Michelangelo and the reactivation of a fault section at the northern part of the Alto Tiberina fault, compute a hydraulic diffusivity of 0.25 m^2/s. Talwani and Acree (1985) found characteristic hydraulic diffusivities of 0.1-10 m^2/s from 22 case studies worldwide, most estimates clustered around 5 m^2/s. The values given in the ES-Tab. 4 can thus be considered reasonable, which strengthens the hypothesis that these earthquakes might have been triggered by pore pressure diffusion.

In order to shed light on the nature of the relation between water level changes of the Montedoglio reservoir and occurrence of earthquakes, we compare earthquake characteristics with hydraulic parameters (Fig. 7). We assume the location error to be 2 km and and employ it to compute potential errors in hydraulic diffusivity (shown as error bars).

From Fig. 7 (left), it is easily visible that there is no simple relationship between hypocentral distance of earthquakes to the reservoir and time of occurrence, as could be expected in case of earthquakes being triggered by pore pressure diffusion in a homogeneous medium. However, it is not possible to infer if this behavior is due to another triggering mechanism involved or the inhomogeneity of crustal properties, e.g. the presence of pathways with higher diffusivity, e.g. preexisting faults.

In (Fig. 7 (middle), there is no simple relationship between hydraulic diffusivity and filling height of the reservoir and, since apart from the seasonal changes, the filling height increases almost monotonously with time, there is no easily recognizable temporal pattern to the hydraulic diffusivity. This may be due to the fact that in our analysis, we do not account for the coupling between elastic response of the subsurface due to loading of the reservoir and pore pressure diffusion. Loading of the reservoir results in stress changes in the subsurface, which may influence the hydraulic diffusivity. A stress-dependency of hydraulic diffusivity has for instance been observed from repeated injection-flow experiments in mines (G. Manthei, pers. commun.).

The change of hydraulic diffusivity with distance (Fig. 7, right) is interesting, though. Whereas at distances between 2 - 4 km, hydraulic diffusivity is small (0.3 - 1 m^2/s), it shows slightly higher values at distances from 6 - 10 km (2.3 - 4 m^2/s). Especially, there is a group of events at 5 km distance that show significantly higher values of hydraulic diffusivity (7.3 - 8.5 m^2/s), which could hint to a high-permeability connection between reservoir and hypocenters (Fig. 8). However, if the spatial distribution of earthquakes is taken into account, these events do not cluster as closely as expected and are distributed rather parallel to the lake shore, which makes a hydraulic connection unlikely.

On the other hand, these earthquakes occurred within a few hours of each other. Since they have similar magnitudes, they rather constitute a swarm than a shock-aftershock sequence, so their relatively large scatter in space might be questionable. Depending on the actual location error, the hypocentral distribution of these earthquakes could change. For example, the close-by Umbria-Marche fault system could represent a hydraulic connection. However, without relocation of events, such an interpretation remains highly speculative.

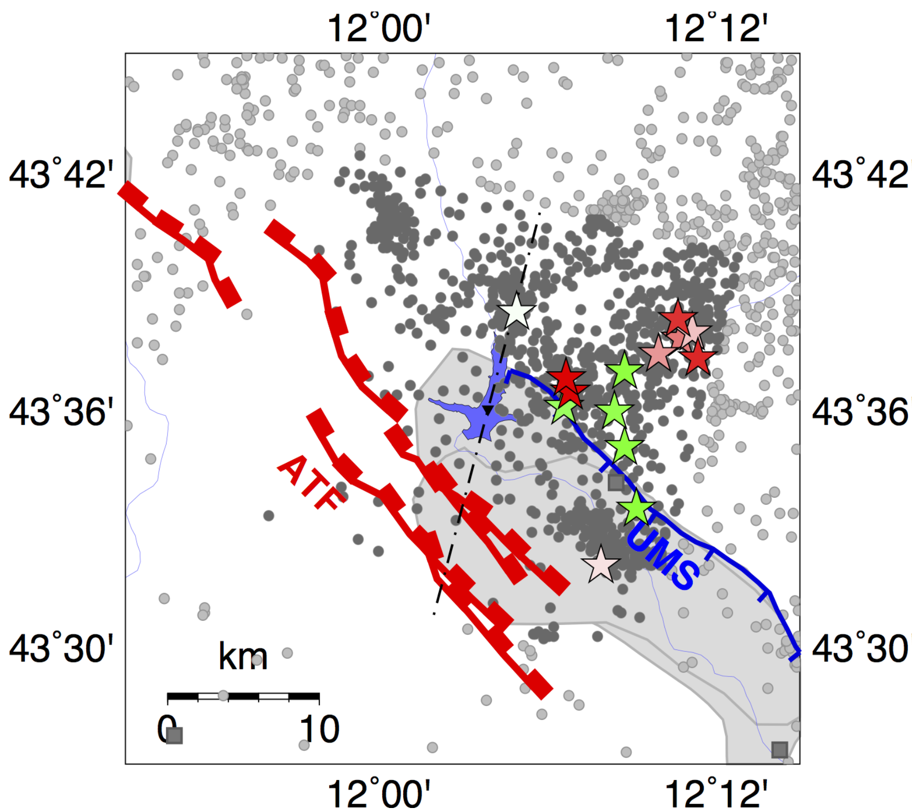

Figure 8: Spatial distribution of seismic hydraulic diffusivity values; stars: distribution of larger magnitude earthquakes, for which hydraulic diffusivity has been computed (for values see the ES-Tab. 4, color scale is identical to Fig. 7). Background: light gray circles: local seismicity recorded since 1983; dark gray circles: local seismicity located within defined 20 km x 20 km area; dash-dotted black line: symmetry axis of 20 km x 20 km area through the Montedoglio reservoir; black triangle: mid-point.

We conclude that diffusion of pore pressure changes resulting from changes of the reservoir water level are likely, but such a simple analysis is not definitive. Instead, future modeling of time-dependent pore pressure, preferably including the coupling between diffusion and deformation processes (e.g. Wang and Kümpel, 2003), will help to assess the potential triggering mechanism.

3.3. Historical seismicity at the geothermal field of Mt. Amiata

In Italy, geothermal exploitation is realized in the Central Italy (Tuscany) at the geothermal fields of Larderello, where the magmatic intrusion became arrested in the crust, and the volcano of Mt. Amiata, where during the superior Pleistocene (400 - 200 ky ago) eruptive activity formed a volcanic edifice with an altitude of 1738 m. Here the formerly governmental enterprise ENEL-Greenpower produces respectively 1.5% of the national energy demand and 23.5% of the energy consumed in Tuscany (Braun et al., 2016).

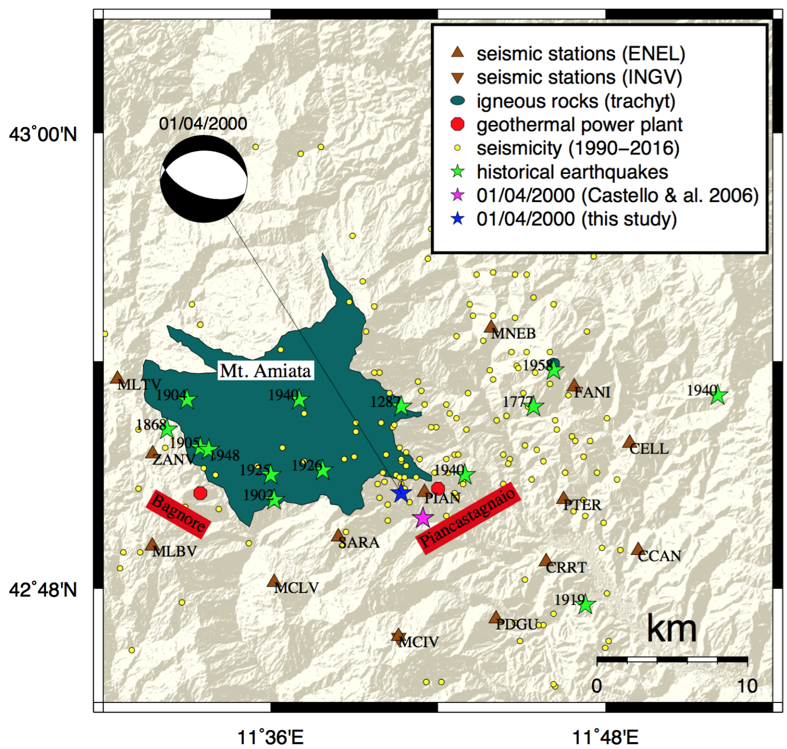

Figure 9: ENEL-seismic network (brown triangles), geothermal power plants (red points), instrumental seismicity reported by ISIDe (yellow dots), historical earthquakes from CPTI (green stars) and epicenters of the 1^{st} April 2000 event reported by (Castello et al., 2006) (purple star) and calculated in the present study (blue star), with corresponding focal mechanism.

Compared to the Apennines, the microseismicity recorded by the INGV-seismic network in the Tuscan geothermal areas is rather low. The yellow dots plotted in Figure 1 represent the only 140 micro-earthquakes with $M \geq 1.5$ reported by (ISIDe – working group, 2016) during the last 25 years, inside a radius of 15 km around Piancastagnaio (PIAN in Fig. 9).

The local seismic network installed in 1982 on Mt. Amiata (by ISMES) - and taken over 10 years later by ENEL-Greenpower (Fig. 9) - recorded 2600 local events in the same time period; 2461 events of those had a magnitude of $M_L < 2$ and were below the level of human perception. This large difference of located earthquakes (factor $>$ 15 - 20) is due to the sparse station density of the INGV-network in the area and was experienced also with a local seismic network in a nearby geothermal area (Braun et al., 2018).

Concerning the microseismicity occurring beneath Mt. Amiata, Mazzoldi et al. (2015) reported that mainly two types of seismic waveforms are observed:

A) the majority of recorded seismic events are local *tectonic events*, characterized by an impulsive arrival of P- and S-waves, $\mathrm{T_{s-p}}$ travel time differences of 0.6 - 2.0 s (corresponding to an epicentral distance of less than 20 km) and a relatively wide spectral range (2 - 20 Hz) (Fig. 10);

B) 5% of the recorded waveforms have been classified as *hydrofracture events*, characterized by a longer duration (20 - 40 s), an incipient 3 - 5 s long high-frequency phase (15 - 20 Hz), followed by a harmonic oscillation of longer duration (25 - 30 s) interpreted as hybrid events (Fig. 10).

The distinction of tectonic- and hybrid or low-frequency events recalls the A-type and B-type classification of volcano-seismic events by Minakami (1960). For the present contribution, ENEL-Greenpower made available the seismograms of the same events analyzed by Mazzoldi et al. (2015) that allowed us to recalculate the respective hypocenters and magnitudes. Fig. 10 show seismic traces and corresponding spectrograms of the B-type and A-type event with the same time scale.

The two event types (B, A) confirm the spectral characteristics described by

Mazzoldi et al. (2015), but both their hypocenters, as well as their magnitude differ fundamentally. The high-frequency event (A) has a much lower magnitude (M 1.3) than the hybrid event (M 2.5), and the corresponding source depths for the A and B event are 3.2 km and 12.6 km, respectively.

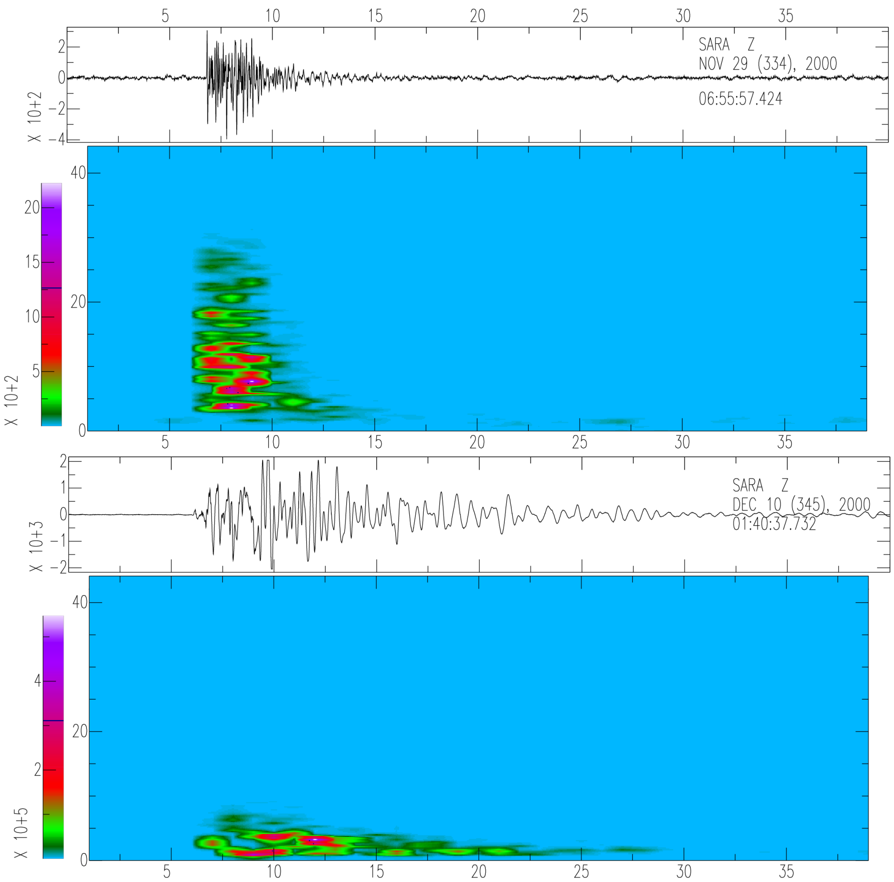

Figure 10: Seismic events recorded by station SARA of the ENEL-network: (top) 29th November 2000, 06:55 UTC: (A-type/tectonic event, after Mazzoldi et al., 2015) M 1.3, Z = 3.2 km; (bottom) 10th December 2000, 01:40 UTC: (B-type/ hybrid event, after Mazzoldi et al., 2015), M 2.5, Z = 12.6 km.

Since the so-called *hybrid event* (B) is located much deeper than the geothermal production level of 3500 m, any relation with geothermal production seems to be unlikely. Hydrofracking as source for the hybrid event-type (B) can be excluded because it is not applied by ENEL; the upper crust is extensively fractured and characterized by high porosity and permeability, such that the reinjected fluids sink already by gravity (Braun et al., 2016).

For seismic events with shallow hypocenters - as e.g. the *tectonic event* of Fig. 10, located close to the geothermal production locations - it is difficult to determine whether the earthquake source is natural or anthropogenic. Generally, fluid depletion from the reservoir may induce elastic stresses in surrounding rock (Dahm et al., 2015), whereas vaporization and reinjection with cold water may lead to thermal stressing of rocks that may also trigger microseismicity (Braun et al., 2016).

Concerning damaging earthquakes striking the Tuscan geothermal areas in the past, the CPTI (Locati et al., 2016) reports some moderate seismic events ($M \leq 5.3$) occurring near Mt. Amiata already before geothermal energy production started (Fig. 9, ES-Tab. 5) underlining that the area is still seismo-tectonically active.

After the beginning of geothermal exploitation, the strongest earthquake of the last 60 years (M_L 3.9/M_w 4.5) in an Italian geothermal area struck the small town of Piancastagnaio on 1st April 2000 (PIAN in Fig. 9), damaging about 50 buildings. Due to the poor available seismic data, only a few publications treat this important seismic event.

Mucciarelli et al. (2001) reported an eccentric damage pattern (towards E) with respect to the reported epicenter, and hypothesized that either the instrumental location was erroneous (reported error 2 - 3 km), a strong rupture directivity, an asymmetric distribution of vulnerable buildings or site effects could be responsible for this observation.

For the present case study ENEL-Greenpower provided a refined 1D velocity model (see ES-Tab.6) - based on seismic prospection data from the geothermal area - in order to relocate the 1st April 2000 earthquake and determine its magnitude. M_L calculated from the ENEL-data and regional broadband data resulted M_L 3.9 and M_w 4.5, respectively, confirming thus the formerly reported values (see Tab. 2). Due to the strong heterogeneity of the crustal velocities beneath the Tuscan geothermal areas and the very limited areal validity of the 1D model of the ES-Tab. 6, the hypocenter location of the 1st April 2000 event was based on P- and S-phases exclusively picked from the ENEL-Amiata seismic network. With respect to the INGV-location (Castello et al., 2006), the new epicenter based on data of the local network is shifted 1.6 km in NW-direction, while depth is well constrained at 3.93 ± 0.64 km.

Origin time	Latitude	Longitude	Depth	Magnitude
18:08:04.328	42.842°N	11.678°E	3.93 km	M_L 3.9, M_w4.5 [*]
18:08:04.000	42.831°N	11.691°E	2.00 km	M_L 3.9, M_w4.5
18:08:05.160	42.939°N	11.733°E	7.50 km	M_D 4.0

Table 2: Hypocentral parameters determined of the 1st April 2000 earthquake after [* this study], by using the seismic data from the ENEL-network and former studies (Castello et al., 2006; Rovida et al., 2016; ISIDe – working group, 2016).

To better constrain the focal mechanism, we included all available P-phase polarities, also those from the other ENEL-networks installed at Mt. Amiata, Latera and Larderello. The obtained focal mechanism shows predominantly normal faulting behavior (Fig. 9). The strike directions of the fault planes result in WNW-ENE and W-E directions, but obviously, main rupture plane and the auxiliary plane cannot be assigned.

In order to control the focal depth, we used an alternative method and an independent dataset from the German seismic array GERESS and compared the synthetic array beam with the beam of the recorded array data. For this purpose, we calculated - for the given epicenter and the focal solution reported in Fig. 9 - synthetic GERESS array-beams for different depths ranging from 1 - 9 km. Fig. 11 shows that the array beam (blue trace) fits the black colored synthetic traces best at a depth of 4.5 km, a value that confirms the result obtained by classical hypocentral location.

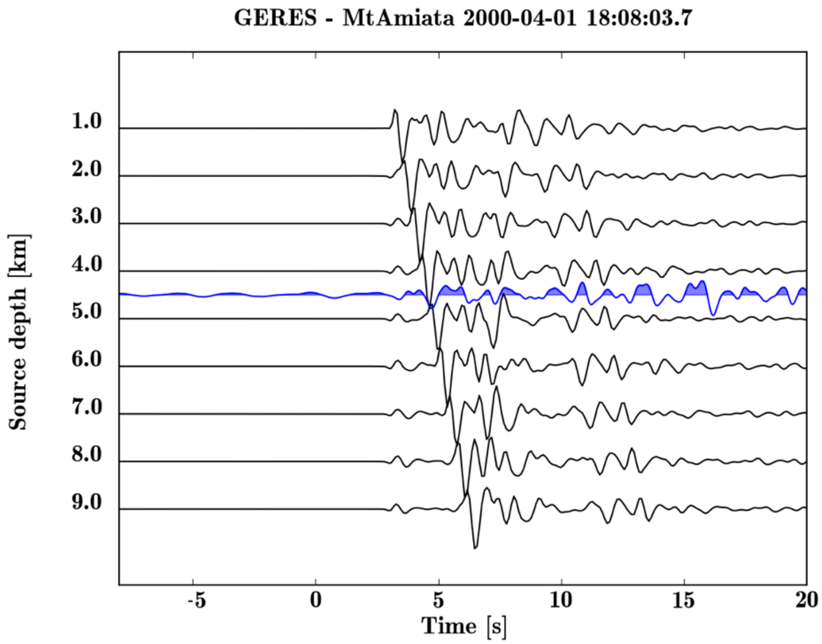

Figure 11: Comparison between observed and predicted waveforms for the GERESS-array (Germany). P and pP phases of the array beam (blue) of the GERESS-Array fitted in the synthetic beams calculated for a depth range of $1 - 9$ km, assuming the focal parameters obtained from the former analysis.

4. Discussion and Conclusion

Many papers have addressed anthropogenic activities and their potential relations with seismicity observed in adjacent areas. The present contribution is, however, a first review of these topics for Italy. Generally, on a short-term time scale, fluid injection rather than by extraction predominantly triggered and induced seismicity. Large fluid volumes introduced in the upper crust as in the case of reservoir impoundment or deep wastewater injection increase the pore pressure lowering the normal stress on the fault. A general question arises about the maximum hypocentral distances that can be ascribed to the influence of such human operations. What is the potential distance range that may be influenced by anthropogenic stress changes? Regarding small volume injections,

like fracking or EGS, the link between injection rate or pressure and seismicity is much more direct and immediate such that the installation of a traffic light system has been proven as an efficient monitoring and alert tool. Since small pore pressure perturbations are directly affecting fault stability, they may trigger earthquakes when fracking is applied near active or preexisting faults. The shallow operation depth of human activity implicates that also small and moderate earthquakes ($M > 3$) can inflict damages on surface structures. For the sparsely populated U.S. midcontinent anthropogenic seismicity caused by as wastewater injection, hydrocarbon recovery or geothermal energy production represents only a minor problem, whereas in most densely populated European countries, similar operations can have a significant impact and may raise strong public concerns. So far, only first steps have been drafted to discriminate induced and triggered from natural seismicity (Dahm et al., 2015).
Hopefully new projects in progress - as the installation of a combination of seismic array and network (Braun et al., 2016) - will shed light on the question of how to discriminate anthropogenic from natural seismicity.

5. Acknowledgements

We would like to commemorate Marco Mucciarelli, who prematurely passed away in 2016. Beyond being a friend and colleague he contributed to the field of induced seismicity with a lot of ideas and initiatives. We are grateful to S. Cola (EAUT) as well as to R. Spinelli and I. Dini (ENEL-Greenpower) for making available their data from the Montedoglio reservoir and Mt. Amiata, respectively. Section 3.1 contains unpublished excerpts of the diploma thesis of our coauthor (A.M-J.) We would like to thank D. Riposati for creating figure 1. The hypocentral distance of events to the lake shore has been estimated using QGIS 2.16 QGIS Development Team (2016) and figures have been prepared employing GMT Wessel et al. (2013). The present research was co-financed by Project INGV-DPC 2014-S2.

6. References

Anelli, L., Gorza, M., Pieri, M., Riva, M., 1994. Subsurface well data in the Northern Apennines (Italy). Mem. Soc. Geol. Ital. 48.

Antonioli, A., Piccinini, D., Chiaraluce, L., Cocco, M., 2005. Fluid flow and seismicity pattern: evidence from the 1997 Umbria-Marche (central Italy) seismic sequence. Geophys. Res. Lett. 32.

Astiz, L., Dieterich, J., Frohlich, C., Hager, B., Juanes, R., Shaw, J., 2014. On the Potential for Induced Seismicity at the Cavone Oilfield: Analysis of Geological and Geophysical Data, and Geomechanical Modeling. Technical Report. Report for the Laboratorio di Monitoraggio Cavone. http://labcavone.it/documenti/32/allegatrapporto-studiogiacimento.pdf.

Barchi, M., Minelli, G., Magnani, B., Mazzotti, A., 2003. Line crop 03: Northern Apennines. Mem. Descr. Carta Geol. d'Italia LXII, 127–136.

Bardainne, T., Dubos-Sallée, N., Sénéchal, G., Gaillot, P., Perroud, H., 2008. Analysis of the induced seismicity of the Lacq gas field (Southwestern France) and model of deformation. Geophys. J. Int. 172, 1151–1162. doi:`10.1111/j.1365-246X.2007.03705.x`.

Batini, F., Bufe, C., Cameli, G., Console, R., Fiordelisi, A., 1980a. Seismic monitoring in Italian geothermal areas I: seismic activity in the Larderello-Travale region., in: Report LBL âĂŤ 11555 Lawrence Berkeley Laboratory (Ed.), Proceedings Second DOE-ENEL Workshop on Cooperative Research in Geothermal Energy, Berkeley, CA, USA. pp. 20 – 47.

Batini, F., Cameli, G., Carabelli, E., Fiordelisi, A., 1980b. Seismic monitoring in Italian geothermal areas II: seismic activity in the geothermal fields during exploitation., in: Report LBL – 11555 Lawrence Berkeley Laboratory (Ed.), Proceedings Second DOE-ENEL Workshop on Cooperative Research in Geothermal Energy, Berkeley, CA, USA. pp. 48 – 85.

Batini, F., Console, R., Luongo, G., 1985. Seismological study of Larderello-Travale geothermal area. Geothermics 14, 255 – 272.

Batini, F., Fiordelisi, A., Moia, F., 1990. Main features of the seismicity in the Monte Amiata and Latera geothermal areas (Italy), in: Abstracts XXII General Assembly European Seismological Commission, Barcelona, Spain. pp. 649–654.

Bischoff, M., Cete, A., Fritschen, R., Meier, T., 2010. Coal mining induced seismicity in the Ruhr Area, Germany. Pure Appl. Geophys. 167, 63–75.

Boccaletti, M., Coli, M., Eva, C., Ferrari, G., Giglia, G., Lazzarotto, A., Merlanti, F., Nicolich, R., Papani, G., Postpischl, D., 1985. Considerations on the seismotectonics of the Northern Apennines. Tectonophysics 117, 7–38.

Boncio, P., Brozzetti, F., Lavecchia, G., 2000. Architecture and seismotectonics of a regional low-angle normal fault zone in Central Italy. Tectonics 19, 1038 – 1055. doi:10.1029/2000TC900023.

Braun, T., Caciagli, M., Carapezza, M., Famiani, D., Gattuso, A., Lisi, A., Marchetti, A., Mele, G., Pagliuca, N., Ranaldi, M., Sortino, F., Tarchini, L., Kriegerowski, M., Cesca, S., 2018. The seismic sequence of May 30 – June 9, 2016, in the geothermal site of Torre Alfina (central Italy) and related variations in soil gas emissions. J. Volcanol. Geotherm. Res. , submitted.

Braun, T., Dahm, T., Krüger, F., Ohrnberger, M., 2016. Does geothermal exploitation trigger earthquakes in Tuscany? Eos 97. doi:10.1029/2016EO053197.

Braun, T., Dahm, T., Kühn, D., 2015. Reservoir induced/triggered seismicity: a review. Seismol. Res. Lett. 86, 729.

Braun, T., Schweitzer, J., Azzara, R., Piccinini, D., Cocco, M., Boschi, E., 2004. Results from the temporary installation of a small aperture seismic array in the Central Apennines and its merits for local event detection and location capabilities. Ann. Geophys. 46, 1315–1324.

Buttinelli, M., Improta, L., Bagh, S., Chiarabba, C., 2016. Inversion of inherited thrusts by wastewater injection induced seismicity at the Val d'Agri oilfield (italy). Sci. Rep. 6. doi:10.1038/srep37165.

Caciagli, M., Camassi, R., Danesi, S., Pondrelli, S., Salimbeni, S., 2015. Can we consider the 1951 Caviaga (Northern Italy) earthquakes as non-induced events? Seismol. Res. Lett. 86, 10pp. doi:10.1785/0220150001.

Caloi, P., 1966. L'evento del Vajont nei suoi aspetti geodinamici. Ann. Geofis. 19, 1–84.

Caloi, P., 1970. How nature reacts on human intervention, responsibilities of those who cause and who interpret such reactions. Ann. Geofis. 23, 283–305.

Caloi, P., De Panfilis, M., Di Filippo, D., Marcelli, L., Spadea, M., 1956. Terremoti della Val Padana del 15âĂŞ16 maggio 1951. Ann. Geofis. 9, 64–106.

Caloi, P., Spadea, M., 1966. Principali risultati conseguiti durante l'osservazione geodinamica, opportunamente estesa nel tempo, di grandi dighe di sbarramento, e loro giustificazioni teoriche. Pubbl. ING 407, 261–286.

Carder, D.S., 1945. Seismic investigations in the boulder dam area, 1940 âĂŤ 1944, and the influence of reservoir loading on local earthquake activity. Bull. Seismol. Soc. Am. 35, 175–192.

Castello, B., Selvaggi, G., Chiarabba, C., Amato, A., 2006. CSI Catalogo della Sismicità Italiana 1981-2002, versione 1.1. Technical Report. INGV-CNT. URL: www.ingv.it/CSI/.

Cesca, S., Braun, T., Maccaferri, F., Passarelli, L., Rivalta, E., Dahm, T., 2013a. Source modeling of the M5-6 Emilia-Romagna, Italy, earthquakes (2012 may 20âĂŞ29). Geophys. J. Int. 193, 1658–1672. doi:10.1093/gji/ggt069.

Cesca, S., Dahm, T., Juretzek, C., Kühn, D., 2011. Rupture process of the 7 May 2001 M_w 4.3 Ekofisk induced earthquake. Geophys. J. Int. 187, 407–413. doi:10.1111/j.1365-246X.2011.05151.x.

Cesca, S., Dost, B., Oth, A., 2013b. Preface to ”triggered and induced seismicity: probabilities and discrimination”. J. Seismol. doi:10.1007/s10950-012-9338-z.

Cesca, S., Grigoli, F., Heimann, S., González, A., Buforn, E., Maghsoudi, S., Blanch, E., Dahm, T., 2014. The 2013 September âĂŤ October seismic sequence offshore Spain: a case of seismicity triggered by gas injection? Geophys. J. Int. 198, 941–953. doi:10.1093/gji/ggu172.

Cesca, S., Heimann, S., Stammler, K., Dahm, T., 2010. Automated procedure for point and kinematic source inversion at regional distances. J. Geophys. Res. 115. doi:10.1029/2009JB006450.

Chiaraluce, L., Chiarabba, C., Collettini, C., Piccinini, D., Cocco, M., 2007. Architecture and mechanics of an active low-angle normal fault: Alto Tiberina Fault, Northern Apennines, Italy. J. Geophys. Res. 112. doi:10.1029/2007jb005015.

Chiodini, G., Cardellini, C., Amato, A., Boschi, E., Caliro, S., Frondini, F., Ventura, G., 2004. Carbon dioxide earth degassing and seismogenesis in Central and Southern Italy. Geophys. Res. Lett. 31. doi:10.1029/2004gl019480.

Collettini, C., Barchi, M., 2003. A low-angle normal fault in the Umbria region (Central Italy): a mechanical model for the related microseismicity. Tectonophysics 359, 97–115.

Dahm, T., 2000. Numerical simulations of the propagation path and the arrest of fluid-filled fractures in the earth. Geophys. J. Int. 141, 623–638.

Dahm, T., Becker, D., Bischoff, M., Cesca, S., Dost, B., Fritschen, R., Hainzl, S., Klose, C., Kühn, D., Lasocki, S., Meier, T., Ohrnberger, M., Rivalta, E., Wegler, U., Husen, S., 2013. Recommendation for the discrimination of human-related and natural seismicity. J. Seis. 17, 197 – 202. doi:10.1007/s10950-012-9295-6.

Dahm, T., Cesca, S., Hainzl, S., Braun, T., Krüger, F., 2015. Discrimination between induced, triggered, and natural earthquakes close to hydrocarbon reservoirs: a probabilistic approach based on the modeling of depletion-induced stress changes and seismological source parameters. J. Geophys. Res. Solid Earth 120. doi:10.1002/2014JB011778.

Dahm, T., Krüger, F., Stammlern, K., Klinge, K., Kind, R., Wylegalla, K., Grasso, J., 2007. The $M_W = 4.4$ Rotenburg, Northern Germany, earthquake and its possible relationship with gas recovery. Bull. Seismol. Soc. Am. 97, 691–704. doi:10.1785/0120050149.

Davies, R., Foulger, G., Bindley, A., Styles, P., 2013. Induced seismicity and hydraulic fracturing for the recovery of hydrocarbons. Mar. Pet. Geol. 45, 171–185. doi:10.1016/j.marpetgeo.2013.03.016.

Davis, R., Selvadurai, A., 1996. Elasticity and Geomechanics. Cambridge University Press, Cambridge, UK.

Deichmann, N., Giardini, D., 2009. Earthquakes induced by the stimulation of enhanced geothermal system below Basel (Switzerland). Seismol. Res. Lett. 80, 784–798.

Deichmann, N., Kraft, T., Evans, K., 2014. Mapping of faults activated by the stimulation of the Basel enhanced geothermal system. Geothermics 52, 74–83.

Ellsworth, W., 2013. Injection-induced earthquakes. Science 341. doi:10.1126/science.1225942.

Evans, K., Zappone, A., Kraft, T., Deichmann, N., Moia, F., 2012. A survey of the induced seismic responses to fluid injection in geothermal and CO_2 reservoirs in Europe. Geothermics 41, 30–54.

Flovenz, O., Agustsson, K., Gudnason, E., Kristjansdóttir, S., 2015. Reinjection and induced seismicity in geothermal fields in iceland, in: Melbourne, A. (Ed.), Proceedings World Geothermal Congress, p. 15.

Gaite, B., Ugalde, A., nor, A.V., Blanch, E., 2016. Improving the location of induced earthquakes associated with an underground gas storage in the Gulf of Valencia (Spain). Phys. Earth. Planet. Int. 254, 46–59. doi:10.1016/j.pepi.2016.03.006.

Giuseppetti, G., Zaninetti, A., Angeloni, P., Mucciarelli, M., Federici, P., 1996. Fifteen years of acoustic emissions and microseismic activity monitoring at the Passante hydroelectric reservoir, in: Proceedings of the 1997 ICOLD Conference, pp. 1007–1024.

Gonzáles, P., Tiampo, K., Palano, M., Cannavò, F., Fernández, J., 2012. The 2011 lorca earthquake slip distribution controlled by groundwater crustal unloading. Nat. Geosci. 5, 763–764. doi:10.1038/ngeo1610.

Grigoli, F., Cesca, S., Priolo, E., Rinaldi, A., Clinton, J., Stabile, T., Dost, B., Garcia-Fernandez, M., Wiemer, S., Dahm, T., 2017. Current challenges in monitoring, discrimination and management of induced seismicity related to underground industrial activities: a European perspective. Rev. Geophys. 55, 310–340. doi:10.1002/2016RG000542.

Gupta, H.K., 1992. Reservoir Induced Earthquakes. volume 64. Elsevier.

Heinicke, J., Braun, T., Burgassi, P., Italiano, F., Martinelli, G., 2006. Gas flow anomalies in seismogenic zones in the Upper Tiber Valley, Central Italy. Geophys. J. Int. 167, 794–806. doi:10.11117j.1365-246X.2006.03134.x.

Hreinsdóttir, S., Bennett, R., 2009. Active aseismic creep on the Alto Tiberina low-angle normal fault, Italy. Geology 37, 683–686.

ICHESE, 2014. International Commission on Hydrocarbon Exploration and Seismicity in the Emilia-Romagna region, Report on the hydrocarbon exploration and seismicity in Emilia Region. Technical Report. Regione Emilia-Romagna, E-R Ambiente, Geologia, sismica e suoli. Bologna, Italy. URL: mappegis.regione.emilia-romagna.it/gstatico/documenti/ICHESE/ICHESE_Report.pdf.

Improta, L., Valoroso, L., Piccinini, D., Chiarabba, C., 2015. A detailed analysis of wastewater-induced seismicity in the Val d'Agri oil field (Italy). Geophys. Res. Lett. 42, 2682–2690. doi:10.1002/2015GL063369.

ISIDe – working group, 2016. Italian Seismological Instrumental and Parametric Database, version 1.0. doi:10.13127/ISIDe10.13127/ISIDe.

ISPRA, 2014. Rapporto sullo Stato Delle Conoscenze Riguardo Alle Possibili Relazioni Tra AttivitĂŹa Antropiche e SismicitĂŹa Indotta/Innescata in Italia. Technical Report. Istituto Superiore per la Protezione e la Ricerca Ambientale, Roma, Italy. Roma. URL: www.isprambiente.gov.it/files/notizie-ispra/notizia-2014/rapporto-sismicita-indotta-innescata-in-italia/Rapporto_sismicita_indotta_innescata_in_italia.pdf. 71 pp.

Kaiser, J., 1950. Untersuchungen über das Auftreten von Geräuschen beim Zugversuch. Ph.D. thesis. Technische Hochschule München.

Kaven, J., Hickman, S., McGarr, A., Ellsworth, W., 2015. Surface monitoring of microseismicity at the Decatur, Illinois, CO_2 sequestration demonstration site. Seismol. Res. Lett. 86. doi:10.1785/0220150062.

Leydecker, G., Grünthal, G., Ahorner, L., 1998. Der Gebirgsschlag vom 13. März 1989 bei Völkershausen in Thüringen im Kalibergbaugebiet des Werratals – Makroseismische Beobachtungen und Analysen. Geolog. Jahrbuch Reihe E.

Lizurek, G., Rudzinski, L., Plesiewicz, B., 2015. Mining induced seismic event on an inactive fault. Acta Geophys. 63, 176–200. doi:10.2478/s11600-014-0249-y.

Locati, M., Camassi, R., Rovida, A., Ercolani, E., Bernardini, F., Castelli, V., Caracciolo, C., Tertulliani, A., Rossi, A., Azzaro, R., D'Amico, S., Conte, S., Rocchetti, E., 2016. DBMI15, the 2015 Version of the Italian Macroseismic Database. Technical Report. Istituto Nazionale di Geofisica e Vulcanologia. doi:10.6092/INGV.IT-DBMI15.

Mazzoldi, A., Borgia, A., Ripepe, M., Marchetti, E., Ulivieri, G., della Schiava, M., Allocca, C., 2015. Faults strengthening and seismicity induced by geothermal exploitation on a spreading volcano, Mt. Amiata, Italia. J. Volcanol. Geotherm. Res. 301, 159–168.

McGarr, A., Simpson, D., Seeber, L., 2002. Case histories of induced and triggered seismicity. Academic Press. volume International Handbook of Earthquake and Engineering Seismology of *International Geophysics Series*. chapter 40. pp. 647–661. Isbn: 0-12-440652-1.

Minakami, T., 1960. Fundamental research for predicting volcanic eruptions. Part I. Bull. Earthq. Res. Inst. Tokyo Univ. 38, 497–544.

Mintrop, L., 1909a. Die Erdbebenstation der Westfälischen Berggewerkschafts-Kasse in Bochum, Teil 1/2. Glückauf 45, 357–366.

Mintrop, L., 1909b. Die Erdbebenstation der Westfälischen Berggewerkschafts-Kasse in Bochum, Teil 2/2. Glückauf 45, 393–403.

Moia, F., Angeloni, P., Cameli, G., Zaninetti, A., 1993. Monitoring induced seismicity around geothermal fields and reservoirs, in: First Egyptian Conference on Earthquake Engineering, Hurgada – Egypt, pp. 1–10.

Mucciarelli, M., 2013. Induced seismicity and related risk in Italy. Ingegneria Sismica 30, 118–125.

Mucciarelli, M., Gallipoli, M., Fiaschi, A., Pratesi, G., 2001. Osservazioni sul danneggiamento nella zona del Monte Amiata a seguito dell'evento del 1 Aprile 2000, in: X Congresso Nazionale "L'ingegneria Sismica in Italia", Potenza-Matera. p. 9.

Nicol, A., Carnea, R., Gerstenberger, M., Christophersen, A., 2011. Induced seismicity and its implications for CO_2 storage risk. Energy Proc. 4, 3699–3706.

Piccinelli, F., Mucciarelli, M., Federici, P., Albarello, D., 1995. The microseismic network of the Ridracoli dam, North Italy: d'agriata and interpretations. Pure Appl. Geophys. 145, 97–108.

Piccinini, D., Piana Agostinetti, N., Roselli, P., Ibs-von Seht, M., Braun, T., 2009. Analysis of small magnitude seismic sequences along the Northern Apennines (Italy). Tectonophysics 476, 136–144. doi:10.1016/j.tecto.2009.04.005.

QGIS Development Team, 2016. QGIS Geographic Information System. Open Source Geospatial Foundation. URL: http://qgis.osgeo.org.

Rovida, A., Locati, M., Camassi, R., Lolli, B., (eds), P.G., 2016. CPTI15, the 2015 Version of the Parametric Catalogue of Italian Earthquakes. Technical Report. Istituto Nazionale di Geofisica e Vulcanologia. URL: http://emidius.mi.ingv.it/CPTI15-DBMI15/query_place/, doi:10.6092/INGV.IT-CPTI15.

Rudzinski, L., Cesca, S., G. Lizurek, G., 2015. Complex rupture process of the March 19, 2013, Rudna mine (Poland) induced seismic event and collapse in the light of local and regional moment tensor inversion. Seismol. Res. Lett. 87, 755–787. doi:10.1785/0220150150.

Saccorotti, G., Piccinini, D., Braun, T., 2011. Narrow-band, transient signals in Central Apennines, Italy: hints for underground fluid migration? Geophys. J. Int. 187, 918–928.

Schweitzer, J., 2001. Hyposat – an enhanced routine to locate seismic events. Pure Appl. Geophys. 158, 277–289. doi:10.1007/PL00001160.

Sen, A., Cesca, S., Bischoff, M., Meier, T., Dahm, T., 2013. Automated full moment tensor inversion of coal mining induced seismicity. Geophys. J. Int. 195, 1267–1281. doi:10.1093/gji/ggt300.

Simpson, D., 1976. Seismicity changes associated with reservoir loading. Eng. Geol. 10, 123–150.

Simpson, D., 1986. Triggered earthquakes. Ann. Rev. Earth Plan. Sci. 14, 21–42.

Stabile, T., Giocoli, A., Lapenna, V., Perrone, A., Piscitelli, S., Telesca, L., 2014. Evidences of low-magnitude continued reservoir-induced seismicity associated with the Pertusillo artificial lake (Southern Italy). Bull. Seism. Soc. Am. 104. doi:10.1785/0120130333.

Talwani, P., 1997. On the nature of reservoir-induced seismicity, in: Seismicity Associated with Mines, Reservoirs and Fluid Injections. Springer, pp. 473–492.

Talwani, P., Acree, S., 1985. Pore pressure diffusion and the mechanism of reservoir-induced seismicity, in: Earthquake Prediction. Springer, pp. 947–965.

Valoroso, L., Improta, L., Chiaraluce, L., Di Stefano, R., Ferranti, L., Govoni, A., Chiarabba, C., 2009. Active faults and induced seismicity in the Val d'Agri area (Southern Apennines, Italy). Geophys. J. Int. 178, 488–502. doi:10.1111/j.1365-246X.2009.04166.x.

Waldhauser, F., 2001. HypoDD – A Program to Compute Double-Difference Hypocenter Locations. Open-File Report 01-113. US Geological Survey.

Waldhauser, F., Ellsworth, W., 2000. A double-difference earthquake location algorithm: Method and application to the northern Hayward fault. Bull. Seismol. Soc. Am. 90, 1353–1368.

Wang, R., Kümpel, H.J., 2003. Poroelasticity: efficient modeling of strongly coupled, slow deformation processes in a multilayered half-space. Geophysics 68, 705–717.

Wessel, P., Smith, W., Scharroo, R., Luis, J., Wobbe, F., 2013. Generic mapping tools: improved version released. Eos, Trans. Am. Geophys. Union 94, 409–410.

Zang, A., Oye, V., Jousset, P., Deichmann, N., Gritto, R., McGarr, A., Majer, E., Bruhn, D., 2014. Analysis of induced seismicity in geothermal reservoirs – an overview. Geothermics 52,, 6–21. doi:10.1016/j.geothermics.2014.06.005.

7. Electronic supplements (ES)

ID	Date	Time	Mag.	Latitude	Longitude	Depth (km)
1	1990-05-08	19:58:28.95	3.3	43.55800	12.15300	5.0
2	1990-05-08	22:33:17.44	3.2	43.60100	12.11000	5.0
3	1990-05-08	22:37:24.18	3.0	43.61600	12.14600	5.0
4	1990-05-08	22:38:33.84	3.2	43.58400	12.14600	5.0
5	1990-05-09	01:23:51.80	3.0	43.59900	12.14000	5.0
6	1997-10-02	19:38:02.25	4.2	43.62970	12.17927	5.4
7	1997-10-02	21:38:42.68	4.1	43.62329	12.16614	6.2
8	1997-10-04	03:28:09.74	3.7	43.63236	12.18612	7.0
9	1997-10-05	10:22:12.77	3.5	43.63802	12.17768	2.9
10	1997-10-10	06:44:31.82	3.3	43.62150	12.18949	2.5
11	2001-11-26	00:56:55.66	4.3	43.60739	12.11385	2.8
12	2001-11-26	12:34:13.48	3.8	43.61306	12.11124	2.9
13	2009-02-13	06:39:13.94	3.0	43.64100	12.08200	4.8
14	2011-01-08	20:16:42.37	2.3	43.54500	12.13200	8.1
15	2011-03-21	16:58:36.44	3.1	43.58000	12.07800	55.1
14	2014-12-21	15:15:28.85	3.6	43.53400	12.13200	8.5

Table 3: (ES): Location and origin time for the largest 16 events since starting the impoundment of the MR

event ID	**time (days)**	**hypocentr. dist.) (km)**	**hydraul. diff.** (m^2/s)	**fill height (m)**
1	43	5.6	8.44	9.86
2	43	5.2	7.28	9.86
3	43	5.5	8.14	9.86
4	43	5.5	8.14	9.86
5	44	5.4	7.67	9.97
6	190	6.1	2.27	11.07
7	190	6.7	2.73	11.07
8	192	7.6	3.48	11.07
9	193	4.1	1.01	11.07
10	198	3.9	0.89	11.07
11	363	3.2	0.33	29.84
12	363	3.3	0.35	29.84
13	61	4.9	4.56	39.17
16	231	8.9	3.97	35.05

Table 4: (ES): Hydraulic diffusivity estimated for the largest seismic events.

date	time [UTC]	$lat°$(N)	$lon°$(E)	I_{MCS}	M_e	location
1287		42.880	11.678	VI-VII	4.93	Abbadia
05/10/1777	15:45	42.880	11.757	VII	5.04	Radicofani
17/06/1868	01:50	42.870	11.538	V-VI	4.51	Arcidosso
17/12/1902	05:21	42.839	11.602	VI-VII	4.86	S.Fiora
07/09/1904	11:30	42.883	11.550	V-VI	4.51	Arcidosso
12/02/1905	08:28	42.862	11.558	VI	4.66	S.Fiora
10/09/1919	16:57:20	42.793	11.788	VII-VIII	5.32	Piancastagnaio
03/09/1925	18:55	42.850	11.600	V-VI	4.51	Abbadia
08/01/1926	09:14	42.852	11.631	VII	4.90	Abbadia
04/02/1940	19:25	42.883	11.617	VI	–	Abbadia
19/06/1940	14:10:09	42.850	11.716	VI	4.77	Radicofani
16/10/1940	13:17:35	42.885	11.867	VII-VIII	5.26	Radicofani
03/11/1948	11:40	42.861	11.563	VI	4.76	M.Amiata
30/05/1958	06:26	42.896	11.769	V	4.28	Radicofani
01/04/2000	18:08:04	42.831	11.691	V-VI	4.57	M.Amiata

Table 5: (ES): Historical earthquakes from CPTI (Locati et al., 2016).

depth (km)	v_p (km/s)	v_s (km/s)
0.000	3.200	1.882
0.300	5.500	3.180
0.500	5.800	3.412
0.800	5.800	3.412
1.000	5.200	3.059
5.500	6.200	3.647
24.000	6.400	3.765
24.000	7.800	4.588

Table 6: (ES): Seismic velocity model (1D) of the crust beneath Mt. Amiata